X-661-74-323

PREPRINT

WHAT IS SPECIAL ABOUT CYGNUS X-1 ?

ELIHU BOLDT
STEPHEN HOLT
RICHARD ROTHSCHILD
PETER SERLEMITSOS

NOVEMBER 1974

GSFC
GODDARD SPACE FLIGHT CENTER
GREENBELT, MARYLAND

WHAT IS SPECIAL ABOUT CYGNUS X-1?

Elihu Boldt
Stephen Holt
Richard Rothschild
Peter Serlemitsos

Goddard Space Flight Center
Greenbelt, Maryland

Preface:

This paper is a transcript of a talk entitled "Black Holes - II: X-Ray Observations" given by one of us (E. B.) at the "International Conference on X-Rays in Space" at the University of Calgary (Canada) August 14-21, 1974. It served as the companion lecture to one by Dr. R. Ruffini (Princeton) entitled "Black Holes - I: Theory". Although the results from several key experiments are reviewed this presentation emphasizes recent work by the Goddard X-ray astronomy group, extending the analysis of our data on Cygnus X-1 beyond the rapid temporal variations reported earlier (Rothschild et al., 1974).

WHAT IS SPECIAL ABOJT CYGNUS X-1?

(BLACK HOLES IN THEORY AND OBSERVATION II: X-RAY OBSERVATIONS)

Elihu Boldt, Stephen Holt

Richard Rothschild* and Peter Serlemitsos

Goddard Space Flight Center
Greenbelt, Maryland

ABSTRACT

Of the eight X-ray sources now known which may be associated with binary stellar systems, Cygnus X-1 is the most likely candidate for being a black hole. The X-ray evidence from several experiments is reviewed, with special emphasis on those characteristics which appear to distinguish Cygnus X-1 from other compact X-ray emitting objects. Data are examined within the context of a model in which millisecond bursts (Rothschild et al., 1974) are superposed upon shot-noise fluctuations (Terrell, 1972) arising from "events" of durations on the order of a second. Possible spectral-temporal correlations are investigated, indicating new measurements that need to be made in future experiments.

INTRODUCTION

A more accurate title for this talk might be "What is Special About Cyg X-1?". For comparison in exploring this, Table 1 lists the eight X-ray sources currently discussed as being members of binary stellar systems. The ordering is according to binary period, ranging from the 4.8 hours for Cyg X-3 to times of about a week or more. All but two

*NAS-NRC Resident Research Associate

TABLE I
X-RAY BINARIES

SOURCE	UHURU INTENSITY		FINEST VARIABILITY (SECONDS)	PULSAR * (2ms–10s)	ENERGY SPECTRUM (2–20 keV)	ABSORPTION (>2 keV)	Mx ($M_\odot$)	OPTICAL MEMBER	ECLIPSING	BINARY PERIOD (DAYS)
	MAXIMUM	RANGE								
CYG X-3 (3U2041+75)	194	≥3	$\sim 10^{3}$	<3%	STEEP	YES	–	–	NO	0.2
HER X-1 (3U1635 +35)	100	≥6	1.24	~80%	FLAT	YES	~1	13-15 MAG. LATE A	YES	1.7
CEN X-3 (3U1118–60)	160	≥20	4.84	~90%	FLAT	YES	0.6–1.1	13 MAG. BOIb	YES	2.1
3U1700–37	102	≥2	$\sim 10^{-1}$	<15%	FLAT	YES	~2	6 MAG. O7f	YES	3.4
SMC X-1 (3U0115–73)	28	≥9	$\sim 10^{2}$	–	FLAT	YES	~1.5	13 MAG. BOIb	YES	3.9
CYG X-1 (3U1956+35)	1175	5	10^{-3}	<5%†	FLAT/STEEP	NO	>3	9 MAG. O9.7 Ib	NO	5.6
VELA X-1 (3U0900-40)	100	10	~1	<15%	FLAT	YES	~1.7	6 MAG. B0.5Ib	YES	9.0
CIR X-1 (3U1516–56)	720	≥20	~1	<3%†	STEEP	YES	–	–	YES	>15 **

* UPPER LIMIT (3σ) TAKEN FROM SPADA et al (1974), EXCEPT FOR CYG X-3 (GSFC FLT. 13.010)

**JONES et al (1974)

† POSSIBLE QUASI-PERIODICITIES GREATER THAN 0.5 SECONDS

of these exhibit pronounced occultations. Of the remaining two Cyg X-3 exhibits a large but smooth variation in intensity for the few keV band, with a well established periodicity (Parsignault er al., 1972; Canizares et al., 1973). Since the spectrum of Cyg X-3 shows severe absorption effects (cf., Bleach et al., 1972)at a few keV and the hard X-ray flux may not be periodically modulated (Baity et al., 1973; Feretti et al., 1974), observed variations are likely to be associated with obscuration of the source. However, for Cygnus X-1, the other non-occulting source, there are no strong absorption effects apparent in the few keV region of the spectrum although there is some evidence for intensity variations with a 5.6 day period (Sanford et al., 1974). Hence, Cyg X-1 may be unique in the sense that it affords us a relatively unobscured view of the accretion process close to the compact object where observable differences between a white dwarf, neutron star and black hole could be most pronounced (Ruffini, 1974).

Of course, our strong interest in Cyg X-1 is motivated by its apparently high mass. If the binary interpretation is correct (cf., Bahcall et al., 1974) and if the distance to the optical member is not vastly overestimated (cf., Margon et al., 1973), this mass is the only one listed in Table 1 which exceeds 3 solar masses, the upper limit for a neutron star (Leach and Ruffini, 1973). Therefore, the interpretation of Cyg X-1 as a collapsed object implies a black hole. Effects which could be supporting evidence for this interpretation are:

1) X-ray emission driven by an accretion process
2) Absence of sustained oscillations in the emission (cf., Leach and Ruffini, 1973)

3) Chaotic fluctuations (cf., Shakura and Sunyaev, 1973) down to the millisecond region for a Schwarzchild metric black hole and to the sub-millisecond region for an extreme Kerr black hole.

The 2-20 keV spectra for the sources listed in Table 1 are characterized as either "flat" or "steep" except for the case of Cyg X-1. This exception is related to the situation that the X-ray emission from Cyg X-1 sometimes exhibits a highly dynamic spectrum in the 2-20 keV band. This is probably indicative of an accretion process with special characteristics of the kind to be explored by further studying spectral correlations with radio emission and optical emission such as the λ 4686 line from He II (cf., Hutchings et al., 1973) in the accreting gas.

Except for the pulsars Her X-1 and Cen X-3, sustained oscillations (i.e., pulsar activity) seem to be absent for all sources listed in Table 1, to the limits indicated. Although an observation of Cir X-1 in 1969 by Margon et al. (1971) detected a 1.5 Hz oscillation present during their 8 second exposure, subsequent observations with UHURU (Jones et al., 1974) and an MIT rocket-borne experiment (Spada et al., 1974) did not see any evidence for a pulsar. However, sporadic flaring on time scales down to about a second were evident, such that low duty cycle quasi-periodicities can not be ruled out. For the case of Cyg X-1, rapid sporadic behavior is most pronounced, manifested by millisecond bursts superposed on large "shot noise" variations that are rich in quasi-periodic behavior at frequencies in the vicinity of 1 Hz. These temporal effects for Cyg X-1 will be exhibited in detail later.

Finally, in comparing the sources listed in Table 1, we should not omit the fact that Cyg X-1 is different from the others in one obvious way that could give us an observational bias in that its peak intensity is the highest of all. However, I should also note that our observation of millisecond bursts from Cyg X-1 (Rothschild et al., 1974) occurred during a rocket-borne experiment when the average intensities observed for Cyg X-3 and Cyg X-1 were within about 20% of each other.

II. SPECTRUM

When Cyg X-1 was first observed with UHURU in late 1970 it showed a much steeper spectrum than had been seen with rocket-borne experiments during a span of several years preceeding 1970. As shown in Figure 1, it was not only unusually steep but a number of sightings on the same day (December 21, 1970) gave clear evidence that this spectrum was highly variable (Schreier et al., 1971). Except for a Goddard observation in September 1970 (Bleach et al., 1972) and an NRL observation in June 1964 (Bowyer et al., 1965), all measurements prior to UHURU were essentially consistent with a non-variable flat spectrum in the few keV region. This relatively stable situation seems to have been restored in March 1971 with the sudden onset of detectable radio emission associated with Cyg X-1. The remarkable correlation between the X-ray and radio transitions is exhibited in Figure 2, which shows how the hard X-ray emission (> 10 keV) increased and lower energy X-ray emission (2-6 keV) decreased when the radio source became evident (Tananbaum et al., 1972).

The average spectral situation for Cyg X-1 observed with UHURU prior to the radio onset may be compared with that obtained almost a year later by examination of the two curves exhibited in Figure 3. All measurements since 1971 that I am aware of indicate a spectrum comparable to the flat one (energy spectral index of about 1/2) in this figure. However, a soft X-ray measurement by Stevens et al. (1972) in October 1971 may be interpreted (Garmire, 1974) in terms of a steep component decreased in intensity from that steep component shown in Figure 3, so that it becomes recognizable only below about a keV. In this way, the amount of interstellar X-ray absorption needed to match the soft part of the spectrum becomes high enough to be compatible with that recently inferred by Ryter et al. (1974) on the basis of interstellar reddening. Since Cyg X-1 may have undergone a radio intensity variation close to the time of the soft X-ray observation in October 1971 (Hjellming, 1973), possible correlations of any steep X-ray spectral component with relatively small radio transitions subsequent to the large one in March 1971 need to be pursued further.

The spectral history of Cyg X-1 is summarized in Table 2 in terms of measurements that bracket most closely in time the known pronounced spectral transitions. The high intensity of Cyg X-1 in the 2-10 keV band observed by NRL in 1964 (Bowyer et al., 1965) was several times higher than that observed in subsequent rocket-borne experiments and comparable to that seen with UHURU just before the transition in March 1971. Some time between the Livermore measurement in November 1968 (Mac Gregor et al., 1970) and the Goddard measurement (Bleach et al.,

TABLE 2

SOME PROMINENT CYG X-I SPECTRAL TRANSITIONS

OBSERVATION	GROUP	SPECTRAL STATE			
		$h\nu < 10$ keV		$h\nu > 10$ keV	
		LOW	HIGH	LOW	HIGH
1964 JUNE	NRL		X		
1965 APRIL	NRL	X			
1967 MAY	MIT				X
JUNE	MIT			X	
1968 NOV	LLL	X			
1969 JUNE	UCSD				X
JULY	UCSD			X	
1970 SEPT	GSFC		X		
1971 MARCH	UHURU		X	X	
APRIL	UHURU	X			X

1972) in September 1970, the few keV spectrum began to steepen. For energies above 20 keV (i.e., the part of the spectrum accessible from balloon-borne observations) two of the sharpest transitions were a three fold decrease from May to June 1967 (Overbeck and Tananbaum, 1968) and a six fold decrease from June to July 1969 (Matteson, 1971). It was not until the UHURU observations during March-April 1971 that a hard X-ray increase was observed, on a comparable time scale, and where we learned of an apparent anti-correlation of the spectral transitions above and below about 10 keV.

III. 5.6 DAY VARIATIONS?

Although there seem to be some variations in the X-ray emission from Cyg X-1 associated with the binary period, the situation is apparently more complicated than it is for the other well established binaries. Figure 4 summarizes observations of Cyg X-1 made with the University College (London) experiment on OAO-Copernicus (Mason et al., 1974), giving the exposure according to the radial velocity phase of the spectroscopic binary HDE 226868 (zero phase corresponds to the secondary on the far side of the primary) as well as the time measured in Julian days. For eight passes through or near zero phase, there were five occasions when the intensity showed a dip lasting an hour or two. For the first four of these events, the measured spectrum indicated increased absorption; the fifth dip associated with zero-phase may be indicative of the chance of an associated coincidence with random intensity fluctuations since this "event" showed no absorption. An OSO-7 experiment (Li and Clark, 1974) examined Cyg X-1 at zero-phase on four occasions

and observed an absorption event once (also shown on Figure 4); the characteristic energy for unit optical depth changed from about 0.6 keV to about 1.9 keV during the dip. So, the score seems to be five clear absorption events out of twelve that would be expected for a strictly regular phenomenon. Furthermore, the OAO observations suggest that these events are not synchronized to zero-phase and may be progressively shifting in phase. In summary, these events are recurrent but not regular, and it appears that while the binary motion in itself is a necessary condition it is not sufficient for their occurrence. Mason et al. (1974) interpret this behavior in terms of a model whereby the observed X-ray emission is intercepted by a variable stream of matter that bridges the primary star and the X-ray source.

The last continuous Copernicus observation of Cyg X-1 shown in Figure 4 corresponds to an interval of 6.5 days in November 1973 which extended through two zero-phase transitions. The overall intensity pattern during this observation suggests a broad maximum centered at phase 0.5, with a maximum to minimum intensity in the ratio 4/3. However, considering a series of zero-phase observations spread throughout the preceeding year, the maximum to minimum intensity is also in the ratio 4/3. I conclude, then, that the suggestion of a 5.6 day periodic intensity variation for Cyg X-1 is in need of more supporting evidence.

VI. FAST FLUCTUATIONS

The difference between Cyg X-1 and other X-ray emitting members of binary systems as regards short-term variations is illustrated in

Figure 5. The figure exhibits samples (15 seconds each) of the count-rate profile for Cyg X-1, Cyg X-3 and Her X-1 obtained during the same rocket-borne Goddard experiment on October 4, 1973 (Rothschild et al., 1974). Even without folding, the raw Her X-1 data clearly show the 1.24 s period pulsar. To within the statistical uncertainties, Cyg X-3 shows no signal variations on any of the time scales examined. In sharp contrast, Cyg X-1 exhibits rapid, large and apparently chaotic fluctuations.

The first high temporal resolution study of Cyg X-1 after the spectral transition of March 1971 was made on May 1, 1971 with a rocket-borne experiment by Rappaport et al. (1971). This observation lasted somewhat over a minute and involved 1 millisecond resolution. The count rate profile for this exposure is shown in Figure 6 and is qualitatively similar to that obtained over two years later in the Goddard experiment. The low frequency portion of the power density spectrum for these MIT data is shown in Figure 7. Although the portion of the spectrum above ~ 1 Hz gave no indication of significant deviations from what would be expected from white noise and rocket motion could make some contribution below ~ 0.2 Hz the remaining region (i.e. between 0.2 Hz and 1 Hz) exhibits so much power that this frequency band alone corresponds to about a 30% modulation of the total signal.

In terms of apparent periodicities, the detailed temporal behavior of Cyg X-1 seems to change from one observation to the next. The discovery of rapid pulsations for Cyg X-1 by Oda et al. (1971) suggested there might be important frequency components up to ~ 14 Hz during

various 20 second duration UHURU exposures. An 8 second rocket observation by Holt et al. (1971) indicated frequency components up to ~ 5 Hz. Subsequent longer duration observations with UHURU (Schreier et al., 1971) indicate no persistent periodicity but the short term presence of many frequencies ranging from ~ 0.1 Hz to ~ 3 Hz and persisting for times on the order of a few seconds. Figure 8 is a sonogram (Oda et al., 1972) of the MIT rocket data (Figure 6) and shows how various frequency components up to ~ 5 Hz (200ms) come and go during that 70 second exposure.

Is this quasi-periodic behavior genuine, indicative of some oscillatory physical process, or is it merely a manifestation of some other type of underlying variation?

V. SHOT-NOISE MODEL

Terrell (1972) examined the UHURU data of Oda et al. (1971) in terms of the fluctuations arising from the superposition of randomly occurring pulses, (i.e. shot-noise). As shown in Figure 9, the computer simulations of the count rate profile based upon a random sample of shot-noise at an average rate of 400 sec^{-1} for pulses of 0.25 second duration each easily replicates the qualitative appearance of the UHURU data.

A key aspect of Terrell's analysis may be seen in Figure 10, where he exhibits the power density spectrum for the computer simulated count rate profile of Figure 9; significant power in excess of that expected for counting statistics alone is clearly evident. The important result is that shot noise adds greatly to power density fluctuations expected from just counting statistics and can actually masquerade as quasi-

periodic behavior in the frequency domain of interest. An elaboration of this effect may be seen in Figure 11 and Figure 12. Figure 11 shows the power density spectra for three UHURU passes at Cyg X-1 and illustrates how, although the dominant frequencies fluctuate from pass to pass, the region of maximum power remains bounded at frequencies less than a few Hz. Figure 12 shows the power density spectra for five of Terrell's computer generated random simulations of data using the same shot noise parameters (i.e., 400 pulses $sec.^{-1}$, 0.25 sec pulse duration) and the temporal resolution and normalization of the UHURU data. Here again, the peak frequencies of significant power fluctuate from trial to trial, but are bounded within a few Hz. The solid curve in Figure 12 gives the average power density spectrum expected for the composite of shot noise and counting statistics and shows how the power increases at the low frequency end. The enhanced fluctuations in power corresponding to this expected average increase appear as significant power when erroneously compared to the power expected from counting statistics alone (i.e., given by the dotted line in Figure 12). This then is an effective mechanism for generating the apparently quasi-periodic behavior seen for Cyg X-1.

An integral measure of shot noise may be obtained by considering the variance in the observed count, as summarized in Figure 13. The shot noise is here parameterized by λ (average pulse rate) and τ (temporal duration of the basic rectangular pulse). The data are represented by noting the counts (N) in each bin (width of ΔT) and constructing the variance $[\overline{(N - \bar{N})^2}]$ and the average $(\bar{N})$. As indicated in Figure 13,

if there is no shot noise the variance per unit bin width is expected to be just the average rate (i.e., $\bar{N}/\Delta T$), independent of ΔT. However, if the data are dominated by shot noise with $\tau \ll \Delta T$, the variance per unit bin width exceeds the average rate by a factor which depends upon λ but is again independent of ΔT. On the other hand, for shot noise dominated data with $\tau \gg \Delta T$ the variance per unit bin width increases from that for the case of no shot noise by a factor which goes linearly with ΔT.

We have calculated the variance per unit bin width for the data of our 50 second exposure to Cyg X-1 as well as the data for Cyg X-3 obtained in the same flight (October 4, 1973) and the results are plotted in Figure 14. Except for statistical fluctuations that vary from the few percent expected for $\Delta T < 0.1$ sec to the tens of percent expected for $\Delta T > 1$ sec., the variance per unit bin width does indeed match the overall average rate for Cyg X-3. On the other hand, for Cyg X-1 the deviation from the mean rate increases significantly with ΔT (for $\Delta T < 1$ sec.) in a manner consistent with the initial linear behavior expected for shot noise. Also, we note that as $\Delta T > 1$ sec. the variance per unit bin width begins to flatten, with variations dominated by statistical fluctuations. The behavior seen here may be characterized by $\lambda = 19$ sec.$^{-1}$ average rate for shot noise pulses of duration $\tau = 1/2$ sec. This corresponds to an average of about 10 shot noise pulses overlapping at any given time, a small enough number to give us an immediate qualitative picture for the large amplitude fluctuations in the Cyg X-1 count rate we observed on time scales comparable to 1/2 sec.

In order to analyze our Cyg X-1 data for quasi-periodic characteristics, the 50 second exposure was divided into 10 second intervals and the principal frequencies were identified. The power density spectra for the band 10 Hz - 1.6K Hz gave no indications of significant deviations from what would be expected from white noise. However, as shown in Figure 15, below 10 Hz there was much significant power for Cyg X-1, especially in the vicinity of 1 Hz. For the threshold power considered here for identifying a principal frequency white noise gives a probability of 0.05 for obtaining an entry anywhere on this plot whereas the number of entries actually exhibited in Figure 15 is over a thousand fold that expectation. A similar analysis for Cyg X-3 exhibits no entries at this power level and gave no indication of significant deviations from what would be expected from white noise anywhere in the power density spectrum.

With the 0.1 Hz resolution corresponding to 10 second intervals of data, several of the principal frequencies shown in Figure 15 for Cyg X-1 appear to persist for consecutive intervals. However, up to frequencies of about 2 Hz there is so much power that about half of the possible frequencies qualify as principal frequencies and the random chance of repitition becomes appreciable. The histogram at the right hand margin of Figure 15 shows the rich concentration of principal frequencies in the band up to about 2 Hz and again illustrates the formidable shot-noise associated background against which one must contrast any frequency in this range that may be a candidate for some genuinely periodic process on time scales $\leq$ 10 seconds.

TABLE 3
CYG X-1 SHOT NOISE PARAMETERS

OBSERVATION	SPECTRAL STATE	PULSE RATE (λ) (SEC^{-1})	PULSE WIDTH (τ) (SECONDS)
1967 SEPT. 7 NRL	(LOW)	10^2	0.3
1970 SEPT. 21 GSFC	HIGH	8×10^2	0.2
1971 MARCH 6 UHURU	HIGH	$(2\text{-}6) \times 10^2$	0.1 – 0.4
1971 MAY 1 MIT	(LOW)	30	0.5
1971 JUNE 11 UHURU	LOW	40	0.3
1973 OCT 4 GSFC	LOW	20	0.5

Adding our results for data obtained in 1973 to those tabulated by Terrell (1972) for observations made through 1971, the shot noise parameters for Cyg X-1 can be traced through its recent history. This is summarized in Table 3, which gives the pulse rate (λ), pulse width (τ), and spectral state measured for Cyg X-1 on six separate occasions during the period 1967-1973. The spectral state is characterized here as being "high" or "low" and refers to the emission below 10 keV, as discussed before. The most remarkable aspect of the evolution so traced is the relative constancy of the characteristic pulse width, at a few tenths of a second, for pulse rates that differ by as much as a factor of forty. On the other hand, the pulse rate appears to be strongly related to the spectral state, where "high" corresponds to higher pulse rates.

VI. PULSED OSCILLATIONS

Since the power spectrum for shot-noise dominated data is equal to the power spectrum for the underlying characteristic shot-noise pulse, we should be able to determine if these pulses carry higher frequency signals than represented by the much lower frequency components at a few Hz that characterize the pulse envelope. In other words, we should be able to tell if we are in fact detecting randomly pulsed oscillations. Since these shot-noise pulses last only a fraction of a second, the inherent resolution in locating carrier frequencies is a few Hz, and "tuning in" involves locating principal frequencies on a time interval comparable to the pulse width.

An analysis of the kind just described was performed on the Cyg X-1 data of Goddard Flight 13.010 and the results are summarized in Figure 16. Principal frequencies above 10 Hz are here indicated for consecutive intervals of 0.3277 s duration, comparable to the underlying shot-noise pulse width, for all of the Cyg X-1 exposure. The frequency grid has a resolution of 3 Hz. For this analysis, the threshold power for defining a principal frequency is such that we expect white noise to exceed this threshold anywhere in the spectrum with a probability of 0.5 for each of the temporal intervals. First, we note that the total number of entries on this plot is consistent with that expected for white noise and that the population of such principal frequencies is statistically consistent with a flat distribution. Even so, the occasional repetition of a principal frequency ($\pm$ 3 Hz) in adjacent intervals could still indicate that a significant "carrier" frequency is sometimes present. However, this sort of repetition in consecutive intervals occurred just once and can not be taken as a statistically significant indication of such an effect.

Figure 16 also shows the average count rate for each of the intervals used for this analysis and it may be of some interest to note that the peak intensity interval, containing three bursts of millisecond duration (Rothschild et al., 1974), exhibited no principal frequencies above 10 Hz. Considering the entire exposure, the 99% confidence upper limit (cf., Holt et al., 1973) to the fraction of the basic shot-noise pulse that may be modulated by frequencies in the band 10 Hz to 1.6 kHz is about 20%.

VII. TEMPORAL-SPECTRAL-INTENSITY CORRELATIONS

To examine possible short-term spectral-temporal effects for Cyg X-1, Brinkman et al. (1974) examined UHURU data in terms of an auto-correlation function. They separately considered two energy bands, 2.1 - 5.1 keV and 5.1 - 12 keV, and the result for the lower energy band observed during a single 50 s pass is shown in Figure 17. The autocorrelation is evaluated at 0.192 s intervals of the time delay parameter. Three features to note are:

1) a rapid decrease in the autocorrelation with the time delay parameter during the first three intervals (i.e. ≤ 0.6 s)
2) a slower less pronounced autocorrelation lasting about fifteen intervals (i.e. ~ 3 s) and
3) possible quasi-periodic behavior for longer times.

Comparing the high and low energy autocorrelation plots obtained from the composite of several sightings Brinkman et al. (1974) noted an asymmetry exhibited in Figure 18. The short-term autocorrelation appears to persist about one time delay interval (i.e. ~ 0.2 s) longer for the low energy band than for the high energy band.

We have examined data from Goddard Flight 13.010 in the same way, using energy bands and time delay intervals as close to those of Brinkman et al. (1974) as readily feasible. The results of this analysis are shown in Figure 19 and are quite comparable to those of Brinkman et al. (1974), including the apparent difference noted between the low and high energy data. For comparison, we looked at the autocorrelation evaluated for the Cyg X-3 data in exactly the same way and obtained

the plots shown in Figure 20, a result to be expected for a flux dominated by statistical fluctuations.

In order to gain some insight into the connection between the autocorrelation behavior and the shot-noise model, we computer simulated a count-rate profile based upon $\lambda = 20$ shot-noise pulses per second of 0.5 s duration each and used these simulated data for the evaluation of the autocorrelation, exactly as done previously for the real data. As shown in Figure 21, this model does a good job of simulating the short-term dominant autocorrelation present for the real data and shows us that the apparent quasi-periodicity in the autocorrelation first noted by Brinkman et al. (1974) is in fact just another artifact of the underlying shot-noise. The simulation was repeated for shot-noise pulses of 0.1 s duration and although the qualitative behavior is similar, a quantitative comparison (i.e., correlation time and apparent frequency of quasi-periodicity) with that for the actual data (i.e., Figure 19) shows that such a small pulse duration is clearly unacceptable. In neither simulation did we get any indication of the longer-term ($\sim$ 3 s) fall-off to the weaker portion of the autocorrelation observed in the Cyg X-1 data.

After comparing our results with those of Brinkman et al. (1974) using the same resolution for the increments of time delay, we repeated the evaluation of autocorrelation using an order of magnitude smaller resolution (i.e., 20.5 ms), and the results are shown in Figure 22. The fast and slow fall-off to the Cyg X-1 autocorrelation are now clearly discernible as two components. The rapid one extrapolates to zero in 0.5 s whereas the slow one goes to zero at approximately 3 s.

As also shown in Figure 22, we used this finer temporal resolution to again computer simulate the autocorrelation behavior. For an assumed shot-noise pulse width of 0.5 s we note that the autocorrelation goes to zero at 0.5 s and then oscillates with an average period of 1 s. Now that we see this simple situation we realize it should have been expected since, after all, the Fourier transform of the autocorrelation is the power density spectrum and, although the frequency spread for a 0.5 s duration pulse is 2 Hz, the dominant frequency component for such a pulse is in fact just 1 Hz.

In order to see how critically tuned the high resolution autocorrelation is to the underlying shot-noise pulse width, we computer simulated two more cases, one for a pulse width of 0.1 s and the other for a pulse width of 0.98 s, and we can see (Figure 22) they are both clearly unacceptable.

We have already noted that the autocorrelation function appears to be a function of energy; both the data of Brinkman et al. (1974) and also our data from Flight 13.010 indicate that the principal portion of the autocorrelation persists somewhat longer ($\sim$ 0.2 s) for the low energy band (2.1 - 5.1 keV) then it does for the higher energy band (5.1 - 12 keV). To pursue this further we have also considered our data above 12 keV, even though the reduced count rate presents some quantum limitation difficulties in computation for the finest resolution (20.5 ms). An intermediate resolution (0.082 s) was used for comparing the autocorrelation at the highest energies ($>$ 12 keV) observed for Cyg X-1 with that for the two lower energy bands (see Figure 23) previously

considered as well as with that evaluated for Cyg X-3, serving as a control. The major result of this analysis is that the principal short-term autocorrelation seems to have disappeared at the highest energies or, if there is a major short-term autocorrelation still present, it is shorter than the temporal resolution used here (i.e., decays away in less than 0.082 s).

In summary, essentially all the temporal variations for Cyg X-1 on time scales from a fraction of a second to minutes and possible longer seem adequately described by shot-noise pulses of about 0.5 s duration, with the admixture of somewhat longer weaker components lasting up to a few seconds. Since the underlying shot-noise pulse width is relatively independent of source intensity we might expect that tracing the longer time scale variations of Cyg X-1 in terms of λ could yield new evolutionary information. That is, the long-time scale behavior should be characterized by the ratio of the variance per unit time to the square root of the mean rate as well as by the average rate itself. Finally, since the shape of the basic shot-noise pulse itself appears to be a function of energy, the need for a more detailed spectral-temporal analysis is clearly indicated. As more data become avaliable we should be able to reconstruct the spectral evolution of these individual events we have referred to as shot-noise pulses and thereby begin to understand their origin(s) and use them as probes of the otherwise inaccessible regions of closest approach to the compact object at the core of Cyg X-1.

VIII. MILLISECOND BURSTS

The characteristic pulses underlying the shot-noise behavior of the Cyg X-1 fluctuations could themselves be the carriers of pronounced fluctuations on a smaller time scale (e.g., millisecond bursts). This kind of sub-structure is suggested by two pieces of evidence. First, we recall that the M.I.T. rocket-borne experiment of 1971 May 1 (see Figure 6) had millisecond resolution; an analysis of that data by Oda et al. (1974) indicates that millisecond fluctuations are "bunched" to a degree that exceeds statistical expectations. Second, for the Goddard experiment (Rothschild et al., 1974) that involved a large enough detection area to identify 8 individually recognizable millisecond bursts during a 50 s exposure 3 of them occurred within an interval of enhanced emission lasting about a third of a second (i.e., a time comparable to a basic shot-noise pulse).

As discussed earlier (see Section VI), a power density spectrum for the Goddard data in the interval of enhanced emission containing 3 of the 8 bursts identified does not yield any principal frequency (10 Hz - 1.6 K Hz) and that implies an upper limit of about 20% to the fraction of this enhanced emission which may be modulated by a periodic signal. To make a meaningful comparison with the observed "burstiness", though, we need to obtain an estimate of the fraction of the emission in this pulse residing in millisecond bursts. In effect, this involves determining how many bursts were actually missed using the rather stringent criterion for statistical significance that was applied to the entire exposure in identifying the 8 bursts already indicated.

To determine the "burst" fraction, we considered an interval of 20 telemetry frames (i.e., ~ 0.4 s) encompassing the enhanced emission region where we found evidence for bunching and divided this into 320 consecutive bins of 1.28 ms duration each. Noting the counts per bin as an independent variable, we obtained a histogram (Figure 24) of the observed population (cf., Boldt et al., 1971). Comparing this distribution with what would be expected from Poisson statistics (also shown in Figure 24), it is quite evident that the 4 bins with counts of 10 or more each are not part of the average population. In fact, the 3 bins of highest count are the ones previously identified as bursts (see Rothschild et al., 1974) and all reside in one telemetry frame (i.e., within an interval of 20.48 ms.). If we eliminate this one telemetry frame from the 20 considered here and compare the resulting "purged" histogram with the now expected Poisson distribution (Figure 25) we see a much improved match. Furthermore, by examining Figure 25 in detail it becomes clear that we are left with a burst of 10 counts per bin and that there may still be anywhere from 0 to 8 more bursts with between 6 to 8 counts per bin remaining, buried in the statistics. For the 4 large unambiguous bursts alone, the burst fraction (i.e., burst counts/ total counts) for the 0.4 s unexpurgated interval considered is 5%. If we add the additional 8 bursts which we might have missed we obtain an upper limit of 13% for this burst fraction.

Now we are ready for the question of periodicity in connection with these bursts. The count rate profile encompassing the telemetry frame containing 3 bursts as well as adjacent frames is exhibited in

Figure 26. We note that the time interval between the first 2 bursts is 5 - 7 milliseconds, comparable to the period expected for the innermost stable orbit around a 12 - 16 $M_\odot$ Schwarzschild metric black-hole. For our present purpose, though, the importance is that we may now restrict our search for periodicities to frequencies within about a 50 Hz band-width at about 170 Hz. And therefore, we may lower our previous estimate of the upper limit to the fraction of enhanced emission modulated by a periodic carrier. However, the 3σ upper limit of 14% so obtained is really no better than the 13% upper limit to millisecond bursting (periodic or not) we obtained by simply extracting "would-be" bursts from the Poisson distribution of fluctuations.

In summary, the fraction of a second "events" dominating the temporal fluctuations (i.e., shot-noise) of Cyg X-1 appear to be correlated with the bunching of millisecond bursts. However, the burst fraction for the one such event clearly indentified is not much greater than about 5% and at most 13 - 14%. And we still can not say much about the question of periodicity except that we seem to be on the threshold of experiments sensitive enough to answer this, perhaps even on the submillisecond time scale to be examined in our current rocket-borne experiment for Cyg X-1.

ACKNOWLEDGEMENTS

It is a pleasure to thank Drs. S. Rappaport, E. Schreier and J. Terrell for valuable suggestions and material included in this review. One of us (E. B.) thanks Dr. D. Venkatesan for his hospitality at the University of Calgary and for the opportunity to prepare this review for the International Conference on X-rays in Space.

REFERENCES

Avni, Y. and Bahcall, J. N. 1974, Ap. J. (Letters), 192, L139. (See Table 1.)

Bahcall, J. N. and Bahcall, N. A. 1973 Solvay Conference. (See Table 1.)

Bahcall, J. N., Dyson, F. J., Katz, J. I. and Paczynski, B. 1974, Ap. J. (Letters), 189, L17.

Baity, W. A., Ulmer, M. P., Wheaton, W. A. and Peterson, L. E. 1973, Nature (Phys. Sci.), 245, 90.

Bleach, R. D., Boldt, E. A., Holt, S. S., Schwartz, D. A. and Serlemitsos, P. J. 1972, Ap. J., 171, 51.

Boldt, E. A., Holt, S. S. and Serlemitsos, P. J. 1971, Ap. J. (Letters), 164, L9.

Bowyer, S., Bryam, E. T., Chubb, T. A. and Friedman, H. 1965, Science, 147, 394. (See Table 2.)

Brinkman, A. C., Parsignault, D. R., Schreier, E., Gursky, H., Kellogg, E. M., Tananbaum, H. and Giacconi, R. 1974, Ap. J. 188, 603.

Bryam, E. T., Chubb, T. A. and Friedman, H. 1966, Science, 152, 66. (See Table 2.)

Canizares, C. R., McClintock, J. E., Clark, G. W., Lewin, W. H. G., Schnopper, H. W. and Sprott, G. F. 1973, Nature (Phys. Sci.) 241, 28.

Garmire, G. P., 1974, Private communication.

Feretti, L., Frontera, R. and Fulgini, F. 1974, preprint (to be published in Ap. Letters.)

Gursky, H. and Schreier, E. 1974, IAU Symposium No. 67. (See Table 1.)

Holt, S. S., Boldt, E. A., Schwartz, D. A. and Serlemitsos, P. J. 1971, Ap. J. (Letters), 166, L65.

Holt, S. S., Boldt, E. A., Serlemitsos, P. J., and Brisken, A. F. 1973, Ap. J. (Letters), 180, L69.

Hjellming, R. M., 1973, Ap. J. (Letters), 182, L29.

Hutchings, J. B., Crampton, D., Glaspey, J. and Walker, G. A. H. 1973, Ap. J. 182, 549.

Jones, D., Giacconi, R., Foreman, W. and Tananbaum, H. 1974, Ap. J. (Letters), 191, L71.

Leach, R. and Ruffini, R. 1973, Ap. J. (Letters), 180, L15.

Li, F. K. and Clark, G. W. 1974, Ap. J. (Letters), 191, L27.

MacGregor, A., Seward, R. and Turiel, I. 1970, Ap. J. 161, 979.

Margon, B., Bowyer, S. and Stone, R. P. S. 1973, Ap. J. (Letters), 185, L113.

Margon, B. Lampton, M., Bowyer, S. and Cruddace, R. 1971, Ap. J. (Letters), 169, L23.

Mason, D. O., Hawkins, F. J., Sanford, P. W., Murdin, P., and Savage, A. 1974, Ap. J. (Letters), 192, L65.

Matteson, J. 1971, Ph. D. Thesis UCSD.

Oda, M., Gorenstein, P., Gursky, H., Kellogg, E., Schreier, E., Tananbaum, H., and Giacconi, R. 1971, Ap. J. (Letters), 166, L1.

Oda, M., Wada, M., Matsuoka, S., Muranaka, N. and Ogawara, Y. 1972, Ap. J. (Letters), 172, L13.

Oda, M., Takagishi, K., Matsucka, M., Miyamoto, S. and Ogawara, Y. 1974, Publ. Astron. Soc. Japan, 26, 303.

Overbeck, J. and Tananbaum, H. 1968, Ap. J. 153, 899.

Parisignault, D. R., Gursky, H., Kellogg, E. M., Matilsky, T., Murray, S., Schreier, E., Tananbaum, H., Giacconi, R. and Brinkman, A. C. 1972, Nature, (Phys. Sci.) 239, 123.

Rappaport, S., Doxsey, R. and Zaumen, W. 1971, Ap. J. (Letters), 168, L43.

Rothschild, R., Boldt, E., Holt, S. and Serlemitsos, P. 1974, Ap. J. (Letters), 189, L13.

Ruffini, R. 1974, Private Communication.

Ryter, C., Cesarsky, C. J. and Audouze, S. 1974, preprint (submitted to Ap. J.)

Sanford, P. W., Mason, K. O., Hawkins, F. J., Murdin, P. and Savage, A. 1974, Ap. J. (Letters), 190, L55.

Schreier, E., Gursky, H., Kellogg, E., Tananbaum, H. and Giacconi, R. 1971, Ap. J. (Letters), 170, L21.

Shakura, N. and Sunyaev, R. 1973, Astron. and Astrophys., 24, 337.

Shulman, S., Fritz, G., Meekins, J. F. and Meidav, M. 1971, Ap. J. (Letters), 168, L49. (See Table 3.)

Spada, G., Bradt, H., Doxsey, R., Levine, A. and Rappaport, S. 1974, Ap. J. (Letters), 190, L113.

Stevens, J. C., Garmire, G. P. and Riegler, G. R. 1972, Ap. J. (Letters), 175, L73.

Tananbaum, H., Gursky, G., Kellogg, E. and Giacconi, R. 1972, Ap. J. (Letters), 177, L5.

Terrell, N. J., 1972, Ap. J. (Letters), 174, L35.

FIGURE CAPTIONS

Figure 1 (a) Spectral density A versus spectral index for a large number of UHURU sightings of Cyg X-1 on 1970 December 21. Dashed line, an approximate fit to the points.
(b) Average spectrum of Cyg X-1 on December 21. Solid lines, best-fit spectral indices to all the points and to the 10-20 keV data separately. Broken lines, typical balloon observation power-law fits. (This figure from Schreier et al., 1971.)

Figure 2 The X-ray intensity of Cyg X-1 in three energy ranges between 2 and 20 keV and the radio fluxes at two frequencies are plotted against the day of 1970 (from Tananbaum et al., 1972).

Figure 3 The average spectra for Cyg X-1 from before and after the 1971 March and April transition, as observed with UHURU (Tananbaum et al., 1972). The spectra are plotted in photons $(cm^2 \text{ sec keV})^{-1}$ versus energy, and various power law fits are labeled with the energy index.

Figure 4 The observing periods of the seven OAO Copernicus observations (Mason et al., 1974) are shown on a plot of radial velocity phase of the spectroscopic binary HDE 226868 versus time. The five Copernicus events are marked with the symbol X (the first four are absorption events). The OSO-7 M.I.T. observation of an absorption event (Li and Clark, 1974) is shown as an error bar corresponding to the estimated precision in establishing the occurrence at zero phase.

Figure 5 The count rate profiles binned every 20.48 ms, for Her X-1, Cyg X-3 and Cyg X-1 during 15-second exposure samples of each source obtained during the same rocket-borne experiment on 1973 October 4 (Rothschild et al., 1974). The inset shows the overall flight profile in counts per 2 second interval versus time after launch (in seconds). The arrows indicate where the 15-second data samples occurred relative to the full exposure.

Figure 6 Cyg X-1 counting-rate profile obtained during an M.I.T. rocket-borne experiment on 1971 May 1 (Rappaport et al., 1971).

Figure 7 The low-frequency portion of the Cyg X-1 power density spectrum for the data described in Figure 6 (Rappaport et al., 1971).

Figure 8 A "Hissagram" (bottom) of the Cyg X-1 data described in Figure 6 (reproduced at top) showing wave amplitudes as a function of wave period and time (i.e. a contoured sonogram) for 2.1 sec samples, obtained by Oda et al. (1972).

Figure 9 A typical set of Cyg X-1 counting-rate data from UHURU (bottom), due to Oda et al., (1971), together with computer-generated shot-noise data (top), due to Terrell (1972). The dashed line indicates a least-squares fit to the triangular trend of the observational data.

Figure 10 Raw, unsmoothed, power spectrum calculated from the shot-noise run shown in Figure 9 (top), showing the large fluctuations at low frequencies typical of shot-noise spectra. The dashed line indicates the spectrum expected for counting statistics alone. (Terrell, 1972).

Figure 11 Power spectra calculated from three sets of data due to Oda et al. (1971), normalized to 1.0 for counting statistics. (Terrell, 1972).

Figure 12 Power spectra calculated from five sets of computer-generated shot-noise including counting fluctuations, normalized to 1.0 for the part of the spectrum due to counting, indicated by the dashed line. The theoretical expectation is shown as a heavy line. (Terrell, 1972).

Figure 13 A scheme for the integral measure of shot-noise parameters.

Figure 14 Variance per unit bin width versus bin width (seconds) evaluated for data from Cyg X-1 (dots) and Cyg X-3 (crosses) obtained in Goddard Flight 13.010 (see Figure 5) on 1973 October 4.

Figure 15 Principal frequencies (i.e. where a priori probability is $\leq 10^{-4}$ for obtaining power density $\geq$ observed value) below 10 Hz for five consecutive 10.486 second intervals of data from Cyg X-1 (Flight 13.010). Right margin presents a histogram of these principal frequencies (scale: 0-5).

Figure 16 Top: Principal frequencies (i.e., where a priori probability is $\leq 10^{-3}$ for obtaining power density $\geq$ observed value) above 10 Hz for consecutive 0.3277 second intervals of data from Cyg X-1 (Flight 13.010). Right margin presents a histogram of principal frequencies in the band 100 - 1500 Hz. Bottom: Counts per 320 microsecond bin (averaged over 1024 bins) versus time (0.2377 second units) corresponding to data intervals used for above power spectral analysis.

Figure 17 The normalized autocorrelation function [$\rho(\tau)$ defined by Brinkman et al. (1974)] for the low-energy bin (2.1-5.1 keV), calculated from the data of a typical UHURU sighting of Cyg 1 on 1971 June 9. The delay time τ is in units of 0.192s. (Brinkman et al., 1974).

Figure 18 The normalized autocorrelation function $\rho(\tau)$ for the low-energy bin (2.1-5.1 keV) and high-energy bin (5.1-12 keV) obtained from the summation of the autocorrelation functions for six UHURU sightings of Cyg X-1. (Brinkman et al., 1974).

Figure 19 The normalized autocorrelation function $\rho(\tau)$, as defined by Brinkman et al. (1974), calculated from the Cyg X-1 data of Goddard Flight 13.010 on 1973 October 4, taken separately for the energy bins 2.1-5.1 keV and 5.1-12 keV. The delay time τ is in units of 0.250s.

Figure 20 The normalized autocorrelation function $\rho(\tau)$ calculated from the Cyg X-3 data of Goddard Flight 13.010, taken separately for the energy bins 2.1-5.1 keV and 5.1-12 keV. The delay time τ is in units of 0.205s.

Figure 21 The normalized autocorrelation function $\rho(\tau)$ calculated from computer generated shot-noise data based upon λ=20 pulses/second of 0.5s duration each, normalized to the average count rate of Cyg X-1 during the exposure of Goddard Flight 13.010. The delay time λ is in units of 0.205s.

Figure 22 The normalized autocorrelation function $\rho(\tau)$ evaluated with 0.0205s resolution for the Cyg X-1 data from Goddard Flight 13.010 and for three sets of computer generated shot-noise data based upon pulse widths of 0.5s, 0.1s, and 0.98s respectively.

Figure 23 (top) The normalized autocorrelation function $\rho(\tau)$ calculated from the Cyg X-1 data of Goddard Flight 13.010, taken separately for the energy bins 2.1-5.1 keV, 5.1-12 keV and 12-35 keV, with a resolution of 0.082s for the delay time.

Figure 23 (bottom) The normalized autocorrelation function $\rho(\tau)$ calculated from the Cyg X-3 data of Goddard Flight 13.010 for the energy bin 2.1-5.1 keV, with a resolution of 0.082s for the delay time.

Figure 24 A histogram of the observed population for the number of counts per 1.28 ms bin during the 409.6 ms duration interval #106 encompassing the peak Cyg X-1 flux during Goddard Flight 13.010. The crosses give the expected Poisson distribution function corresponding to the average rate (2.269 counts per 1.28 ms bin) and the associated statistical rms deviation.

Figure 25 A histogram of the observed population for the number of counts per 1.28 bin during interval #106 of Goddard Flight 13.010, but excluding the 20.48 ms duration frame #7. The crosses give the expected Poisson distribution function corresponding to the average rate (2.082 counts per 1.28 bin) and the associated statistical rms deviation.

Figure 26 Count rate profile (counts per temporal bin) for Cyg X-1 during TM frames #6-8 of interval #106, Goddard Flight 13.010. The telemetry word length of 320 μs is used as the finest resolution temporal bin, and the corresponding data are shown as the shaded histogram for frame #7. The overall histogram shown for frames #6-8 is based on a 1.28 ms bin.

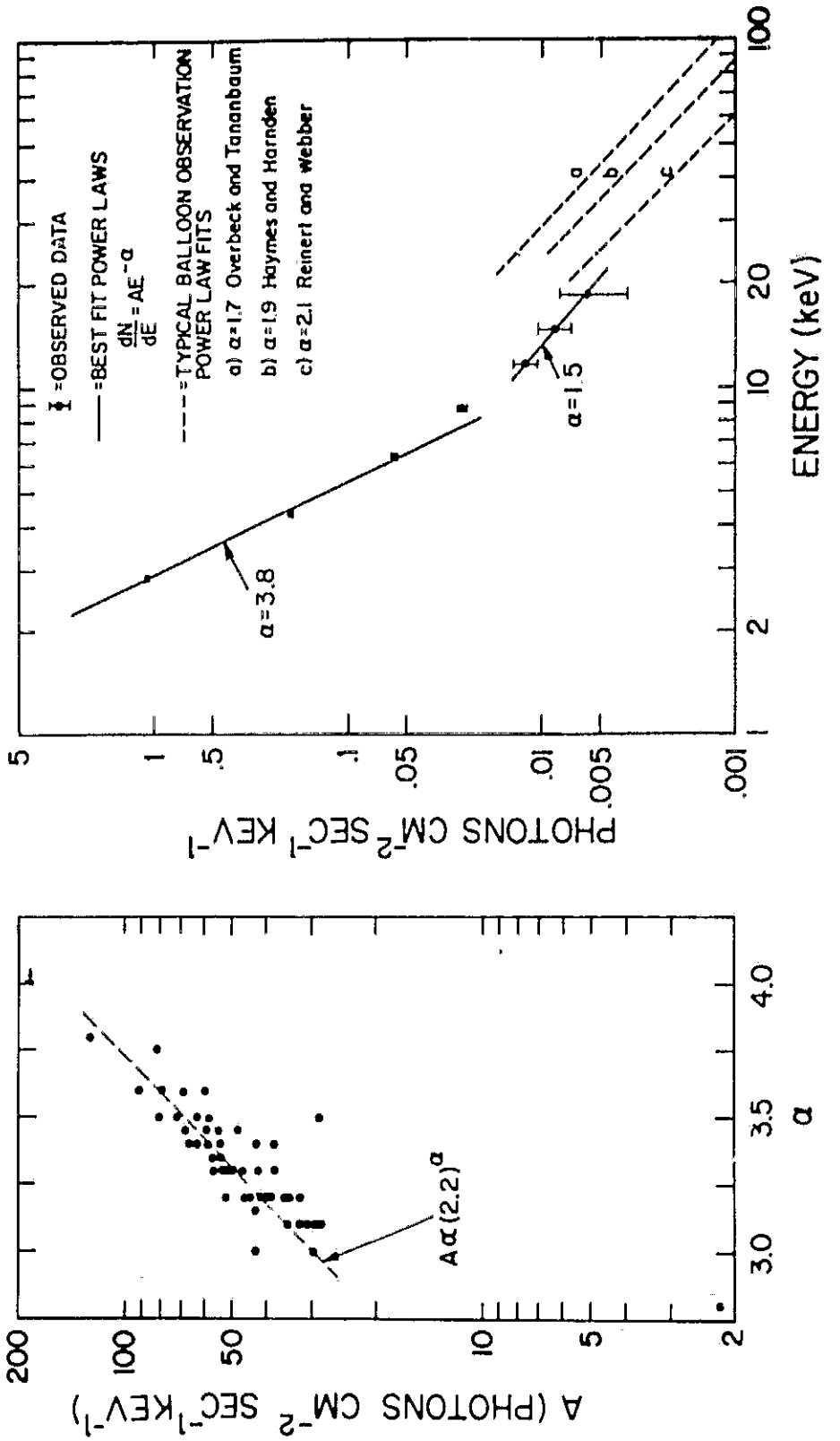
I =OBSERVED DATA
——=BEST FIT POWER LAWS
$\frac{dN}{dE} = AE^{-\alpha}$
- - - =TYPICAL BALLOON OBSERVATION POWER LAW FITS
a) α=1.7 Overbeck and Tananbaum
b) α=1.9 Haymes and Harnden
c) α=2.1 Reinert and Webber
α=3.8
α=1.5
a
b
c
PHOTONS CM^{-2} SEC^{-1} KEV^{-1}
5
1
.5
.1
.05
.01
.005
.001
1
2
10
20
100
ENERGY (keV)
A (PHOTONS CM^{-2} SEC^{-1}KEV^{-1})
200
100
50
10
5
2
Aα(2.2)$^{\alpha}$
3.0
3.5
4.0
α

Figure 1

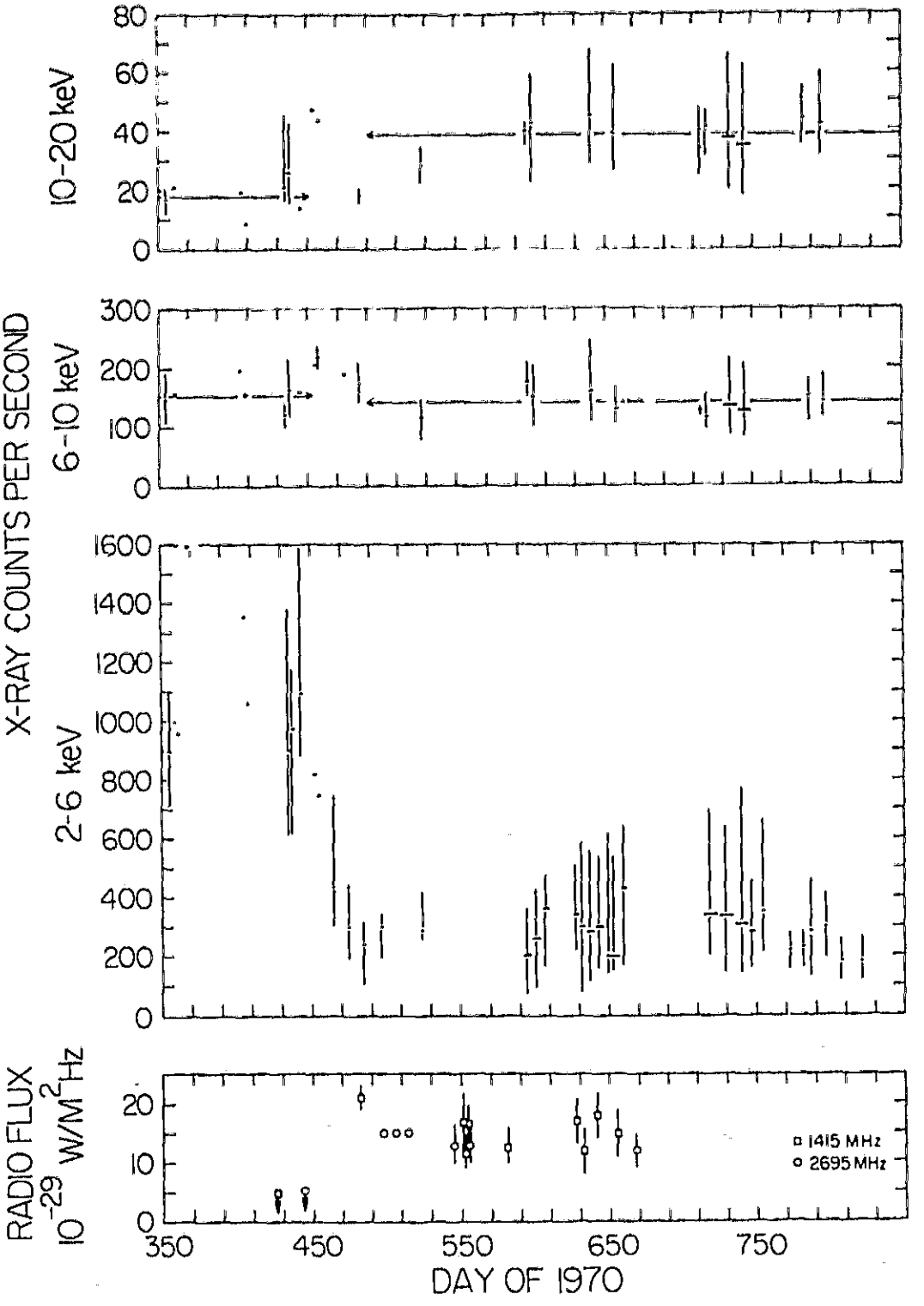
X-RAY COUNTS PER SECOND
10-20 keV
6-10 keV
2-6 keV
RADIO FLUX
10^{-29} W/M^{2}Hz
1415 MHz
2695 MHz
DAY OF 1970

Figure 2

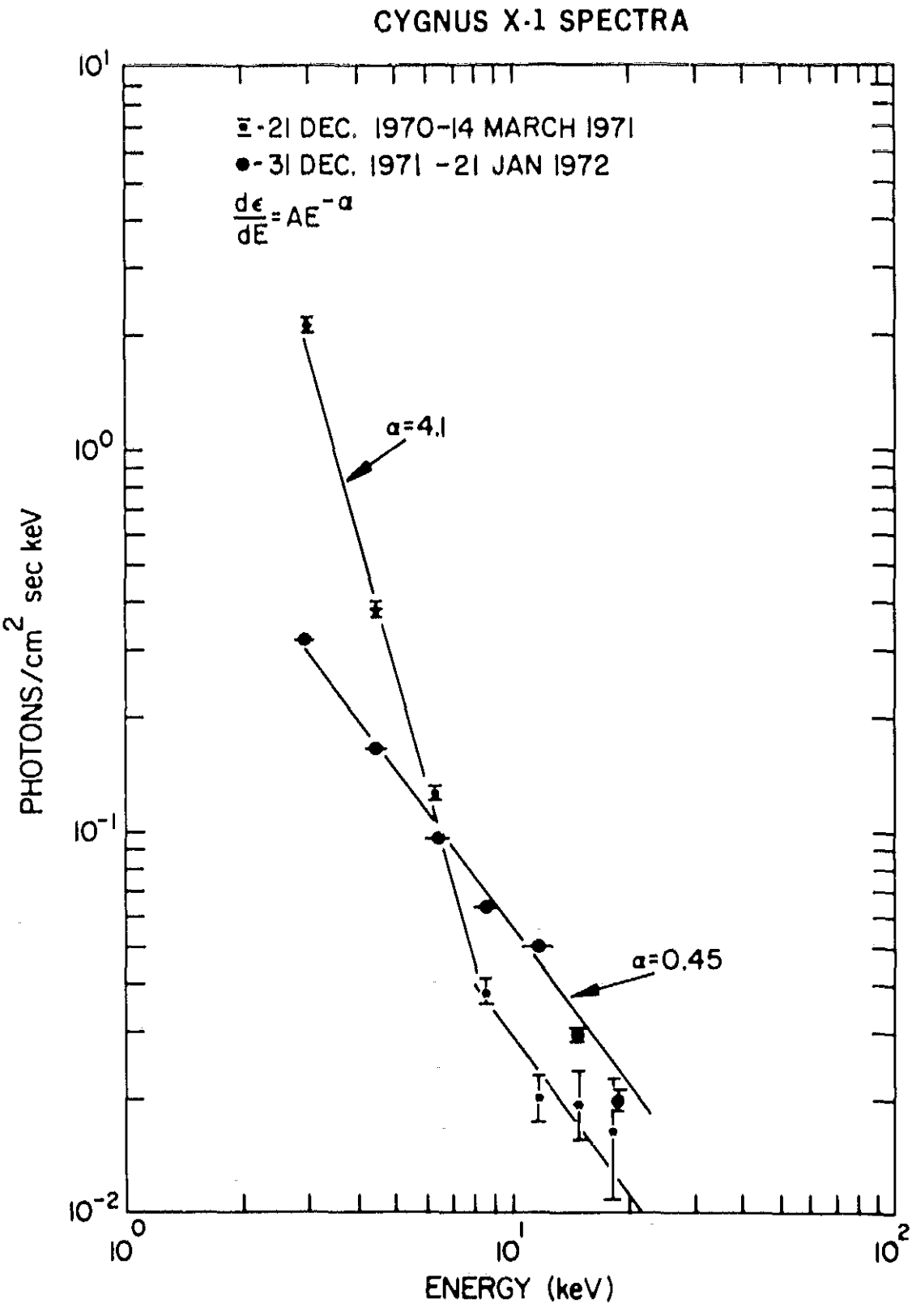
CYGNUS X-1 SPECTRA
⧗ - 21 DEC. 1970 - 14 MARCH 1971
● - 31 DEC. 1971 - 21 JAN 1972
dε/dE = AE^-α
α=4.1
α=0.45
PHOTONS/cm² sec keV
ENERGY (keV)
10¹
10⁰
10⁻¹
10⁻²
10⁰
10¹
10²

Figure 3

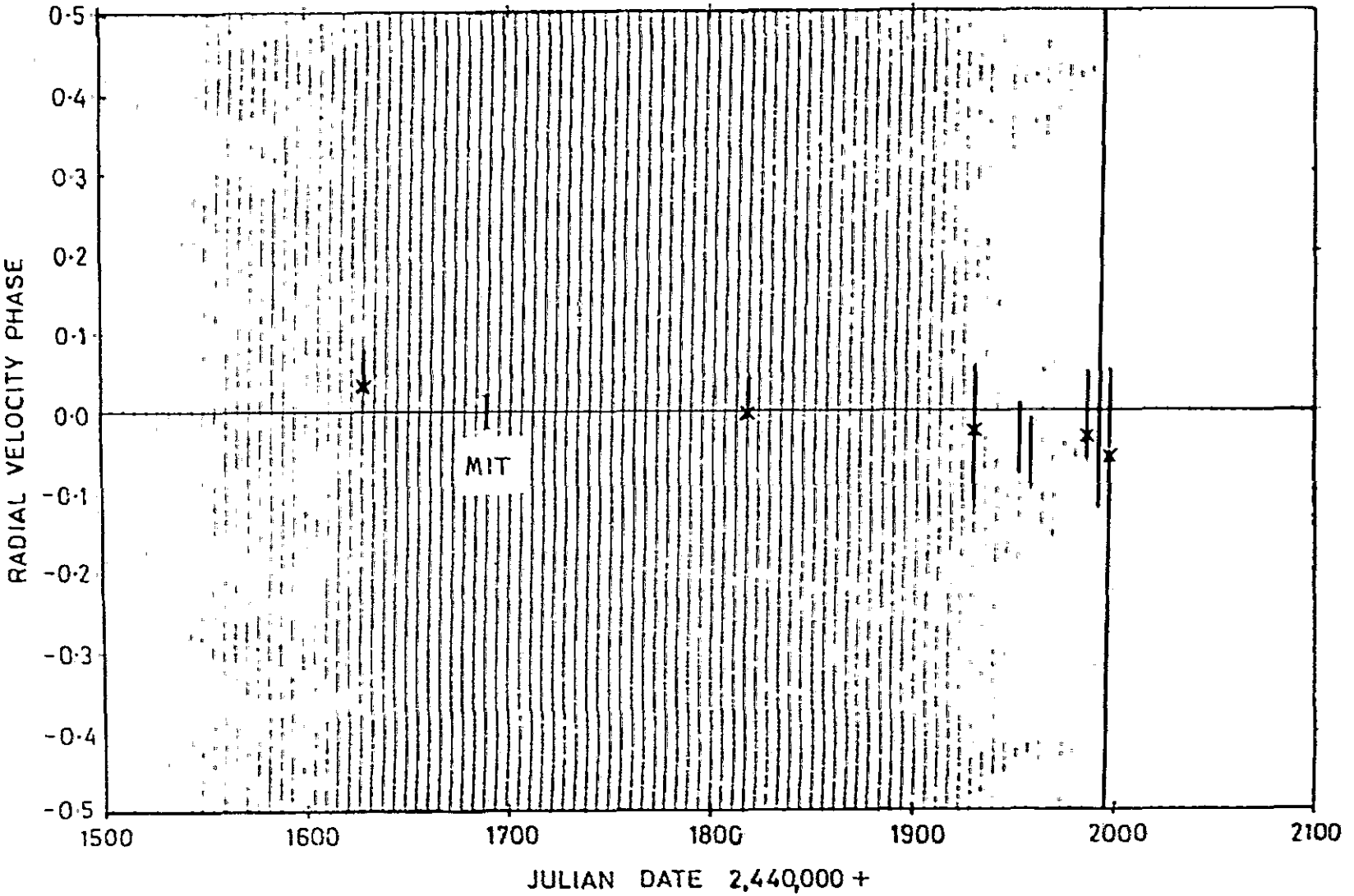
0·5
0·4
0·3
0·2
0·1
0·0
-0·1
-0·2
-0·3
-0·4
-0·5
RADIAL VELOCITY PHASE
MIT
1500
1600
1700
1800
1900
2000
2100
JULIAN DATE 2,440,000 +

Figure 4

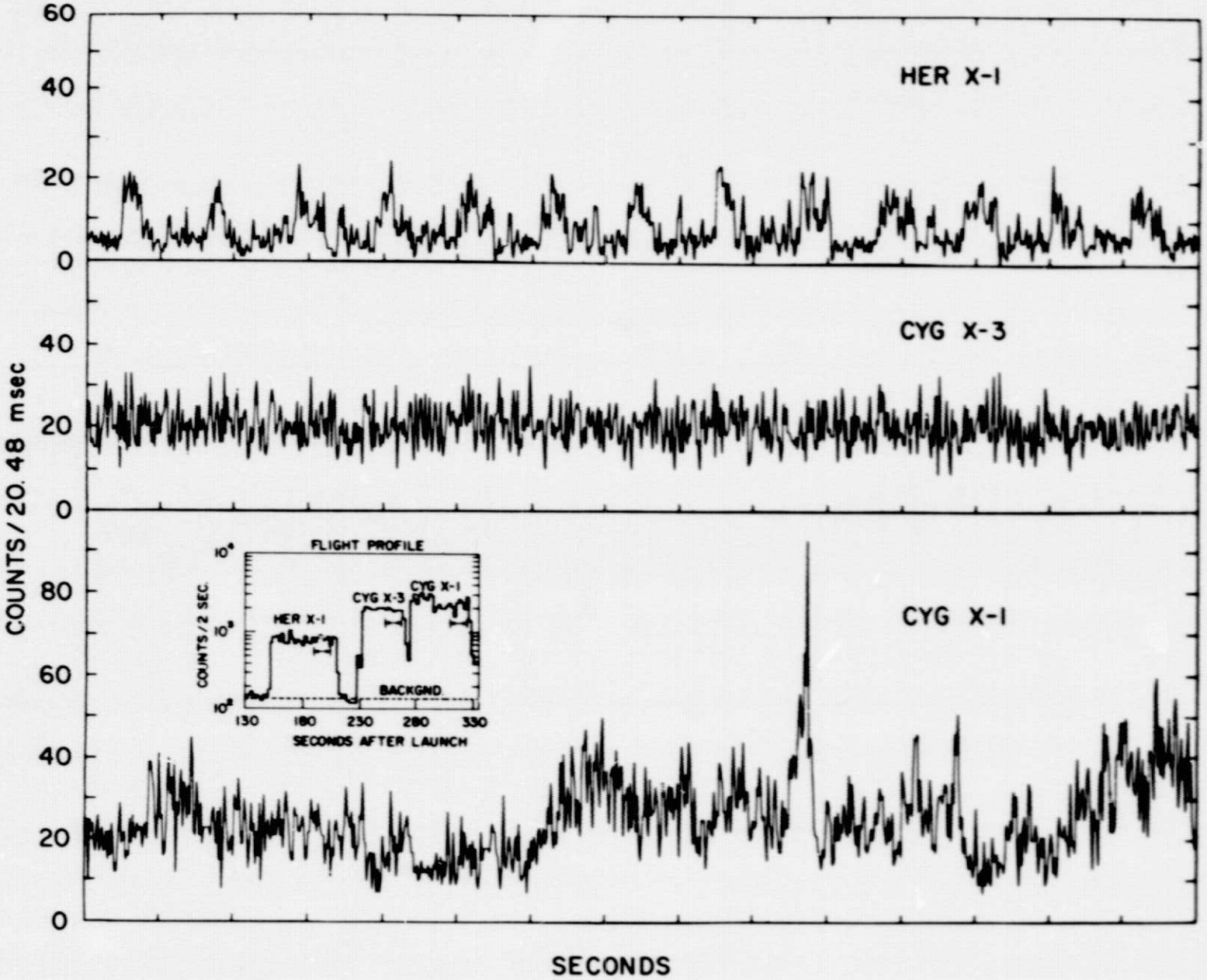
HER X-1
CYG X-3
CYG X-1
COUNTS/20.48 msec
SECONDS
FLIGHT PROFILE
COUNTS/2 SEC.
HER X-1
CYG X-3
CYG X-1
BACKGND
SECONDS AFTER LAUNCH

Figure 5

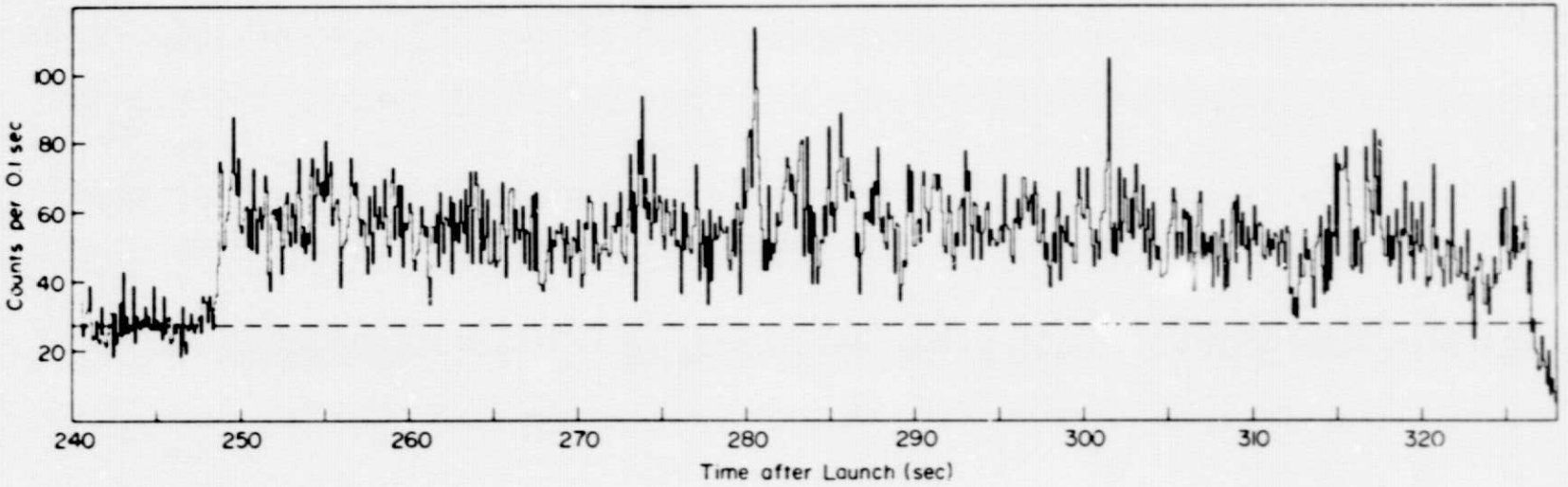
Counts per 0.1 sec
100
80
60
40
20
240
250
260
270
280
290
300
310
320
Time after Launch (sec)

Figure 6

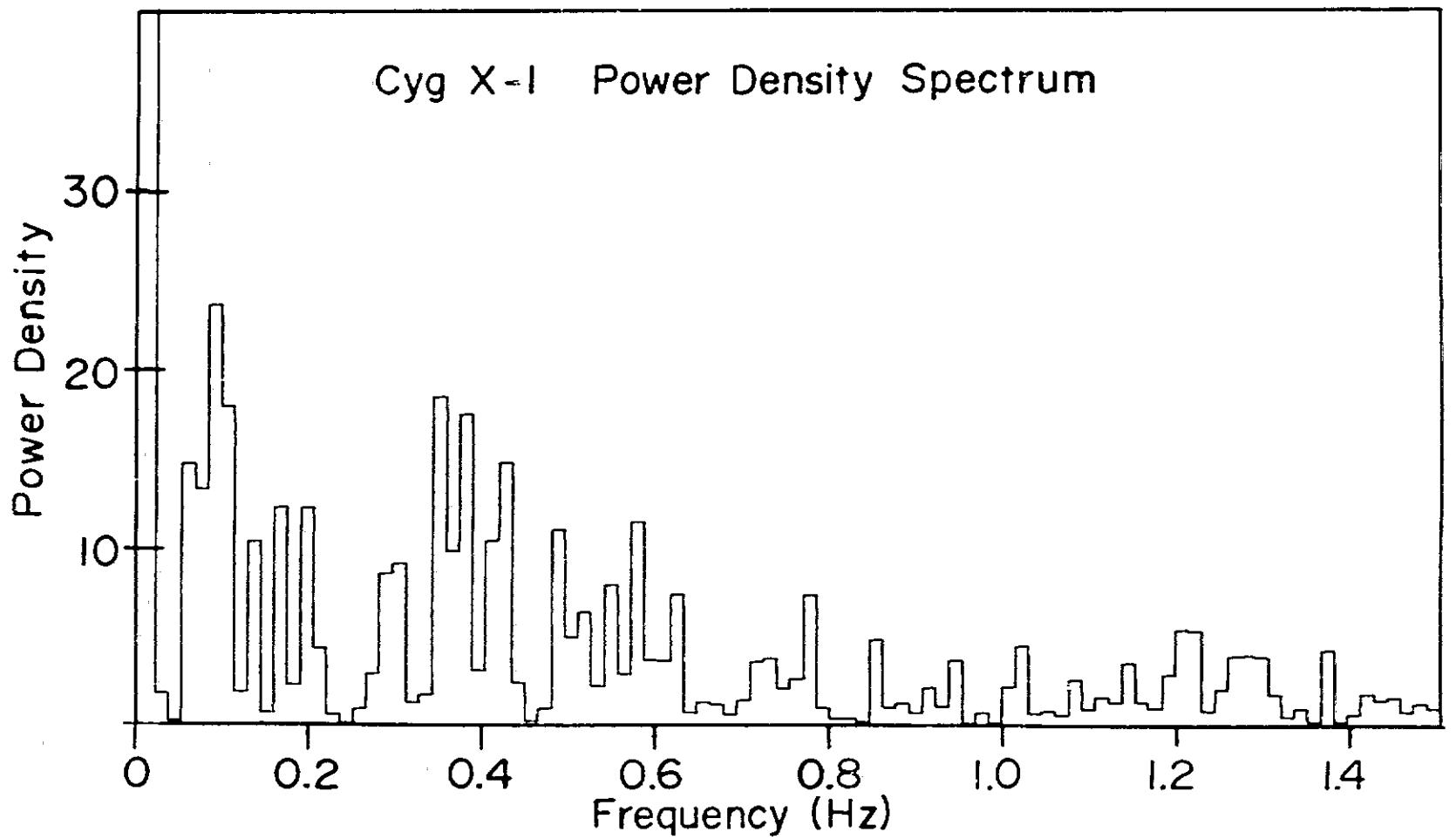
Cyg X-1 Power Density Spectrum
Power Density
30
20
10
0
0.2
0.4
0.6
0.8
1.0
1.2
1.4
Frequency (Hz)

Figure 7

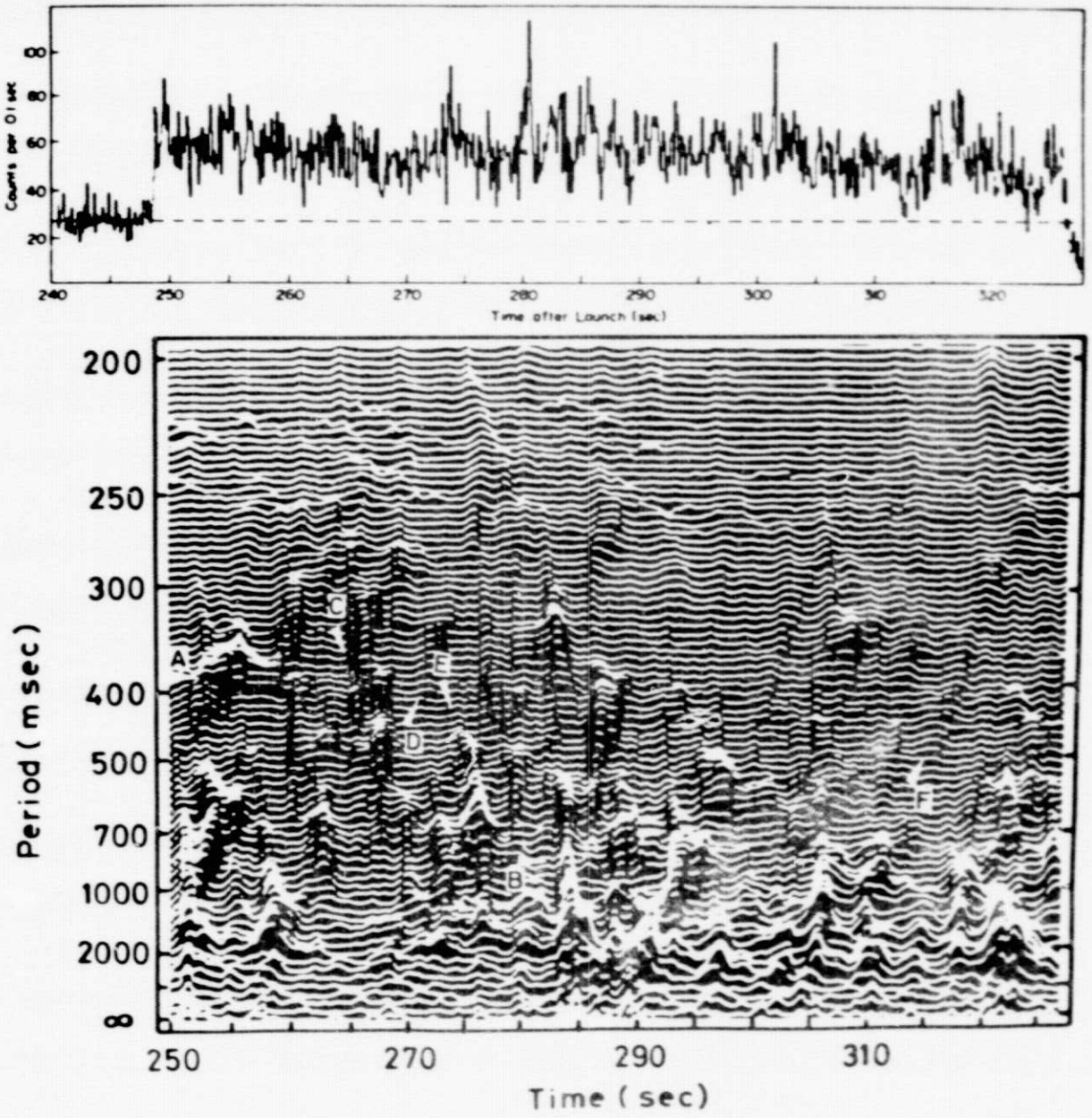
Counts per 0.1 sec
240
250
260
270
280
290
300
310
320
Time after Launch (sec)
200
250
300
400
500
700
1000
2000
∞
Period (m sec)
A
B
C
D
E
F
250
270
290
310
Time (sec)

Figure 8

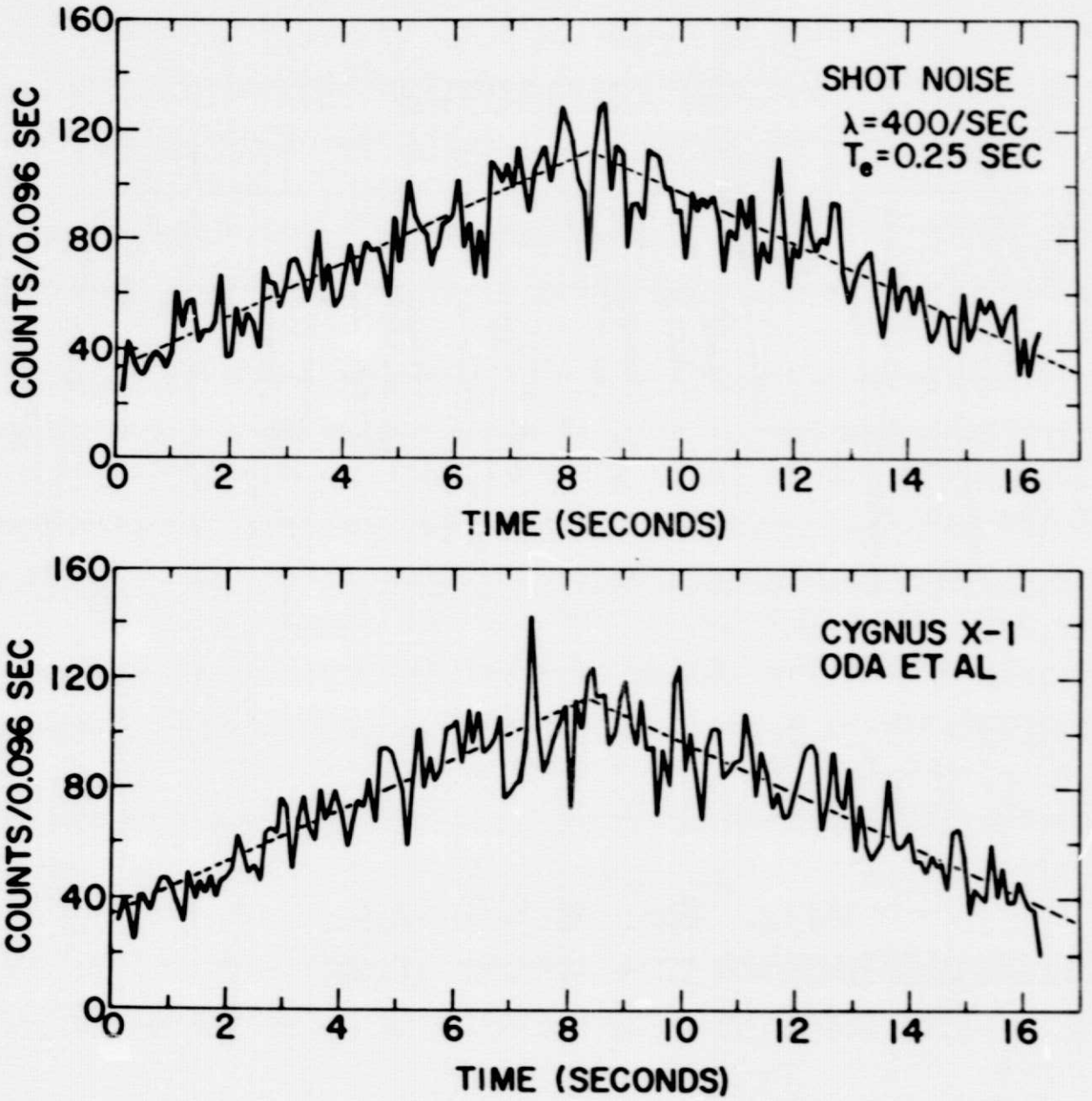
SHOT NOISE
λ=400/SEC
T_e=0.25 SEC
COUNTS/0.096 SEC
TIME (SECONDS)
CYGNUS X-1
ODA ET AL
COUNTS/0.096 SEC
TIME (SECONDS)

Figure 9

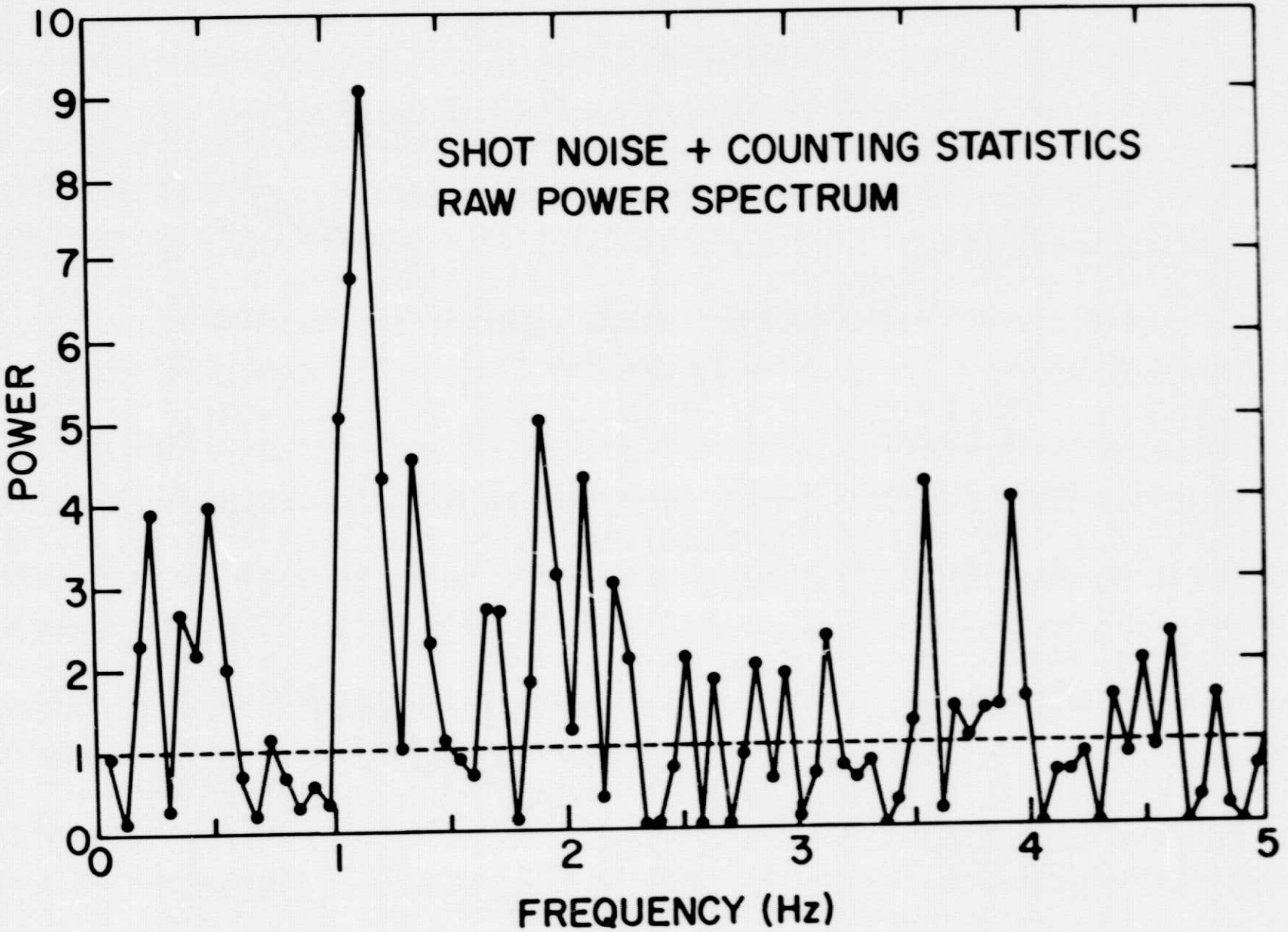
SHOT NOISE + COUNTING STATISTICS
RAW POWER SPECTRUM
POWER
FREQUENCY (Hz)
0
1
2
3
4
5
6
7
8
9
10

Figure 10

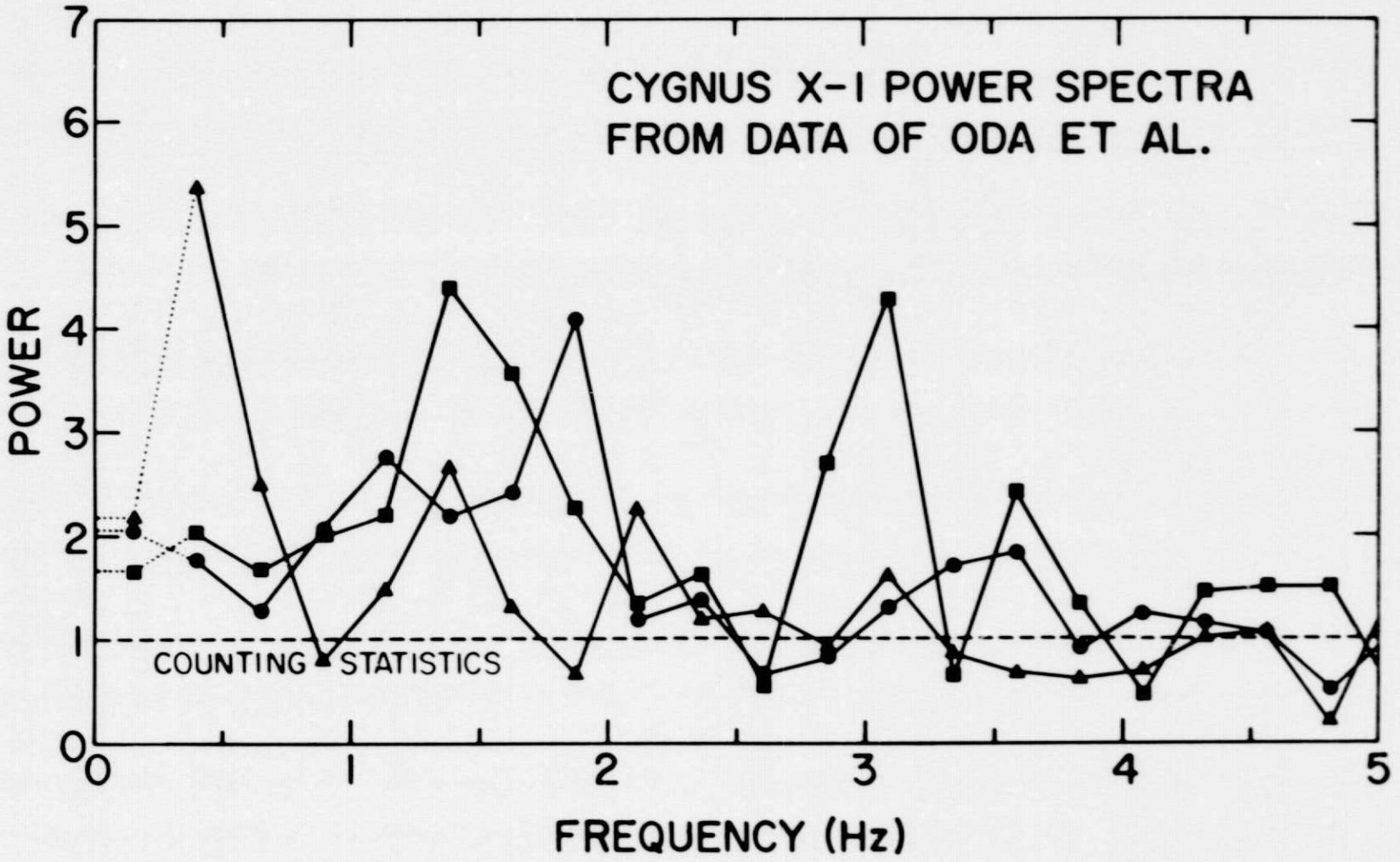
CYGNUS X-1 POWER SPECTRA
FROM DATA OF ODA ET AL.
POWER
FREQUENCY (Hz)
COUNTING STATISTICS
0
1
2
3
4
5
6
7

Figure 11

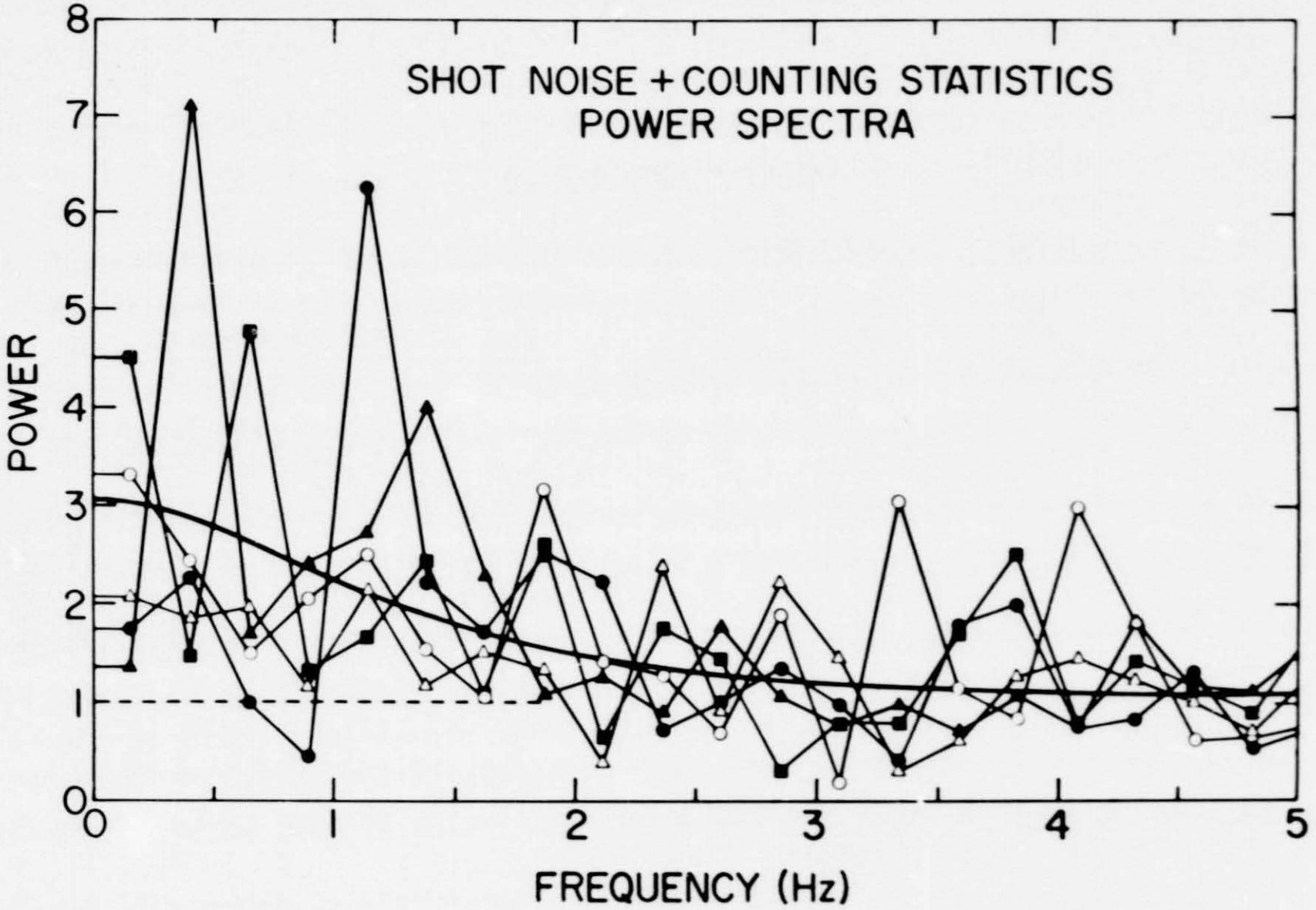
SHOT NOISE + COUNTING STATISTICS
POWER SPECTRA
POWER
FREQUENCY (Hz)
0
1
2
3
4
5
6
7
8

Figure 12

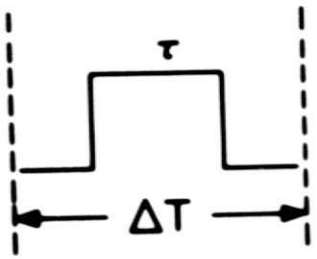

ΔT = DATA BIN WIDTH

τ = PULSE WIDTH (SHOT NOISE)

N = COUNTS IN DATA BIN

λ = SHOT NOISE PULSE RATE

$$\overline{(N-\bar{N})^2}/\Delta T = \begin{cases} (\bar{N}/\Delta T) \text{ (NO SHOT NOISE)} & \\ (\bar{N}/\Delta T)\left[1+\lambda^{-1}(\bar{N}/\Delta T)\,\Delta T/\tau\right] & \Delta T \ll \tau \\ (\bar{N}/\Delta T)\left[1+\lambda^{-1}(\bar{N}/\Delta T)\right] & \Delta T \gg \tau \end{cases} \Bigg\} \text{SHOT NOISE DOMINATED}$$

Figure 13

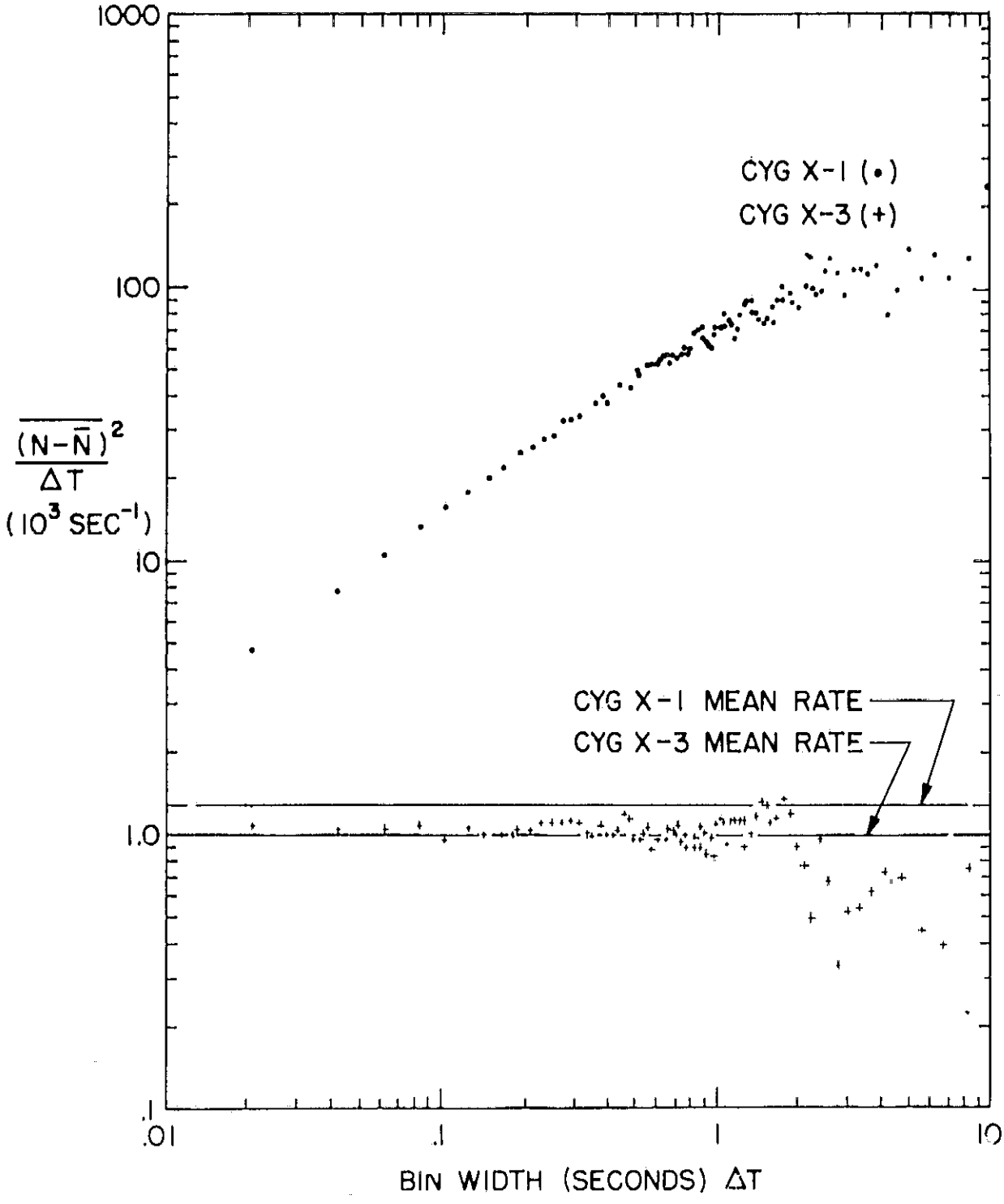
1000
100
10
1.0
.1
.01
.1
1
10
CYG X-1 (•)
CYG X-3 (+)
CYG X-1 MEAN RATE
CYG X-3 MEAN RATE
$\frac{\overline{(N-\bar{N})^2}}{\Delta T}$
(10^3 SEC^{-1})
BIN WIDTH (SECONDS) ΔT

Figure 14

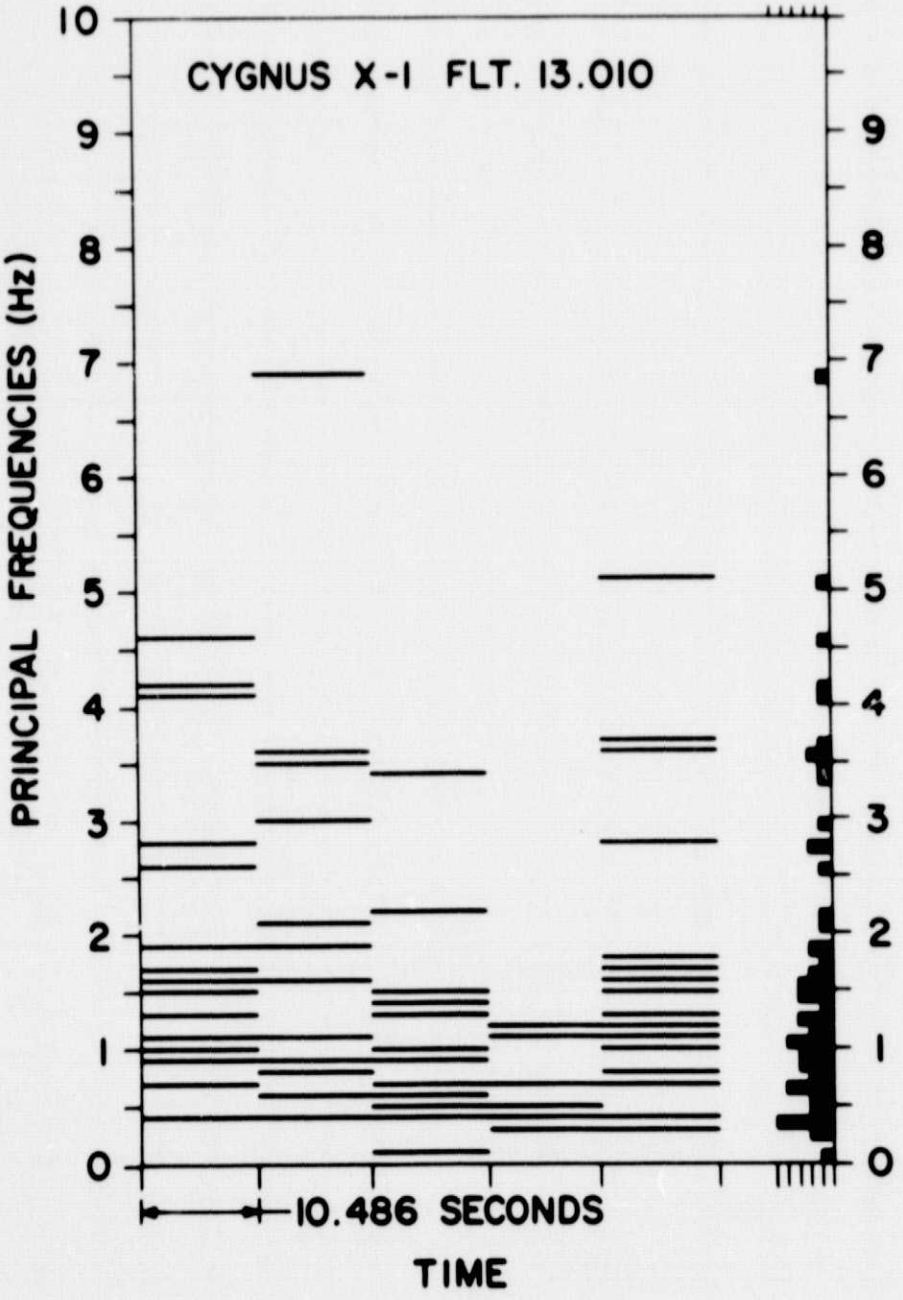
CYGNUS X-1 FLT. 13.010
PRINCIPAL FREQUENCIES (Hz)
10
9
8
7
6
5
4
3
2
1
0
10.486 SECONDS
TIME

Figure 15

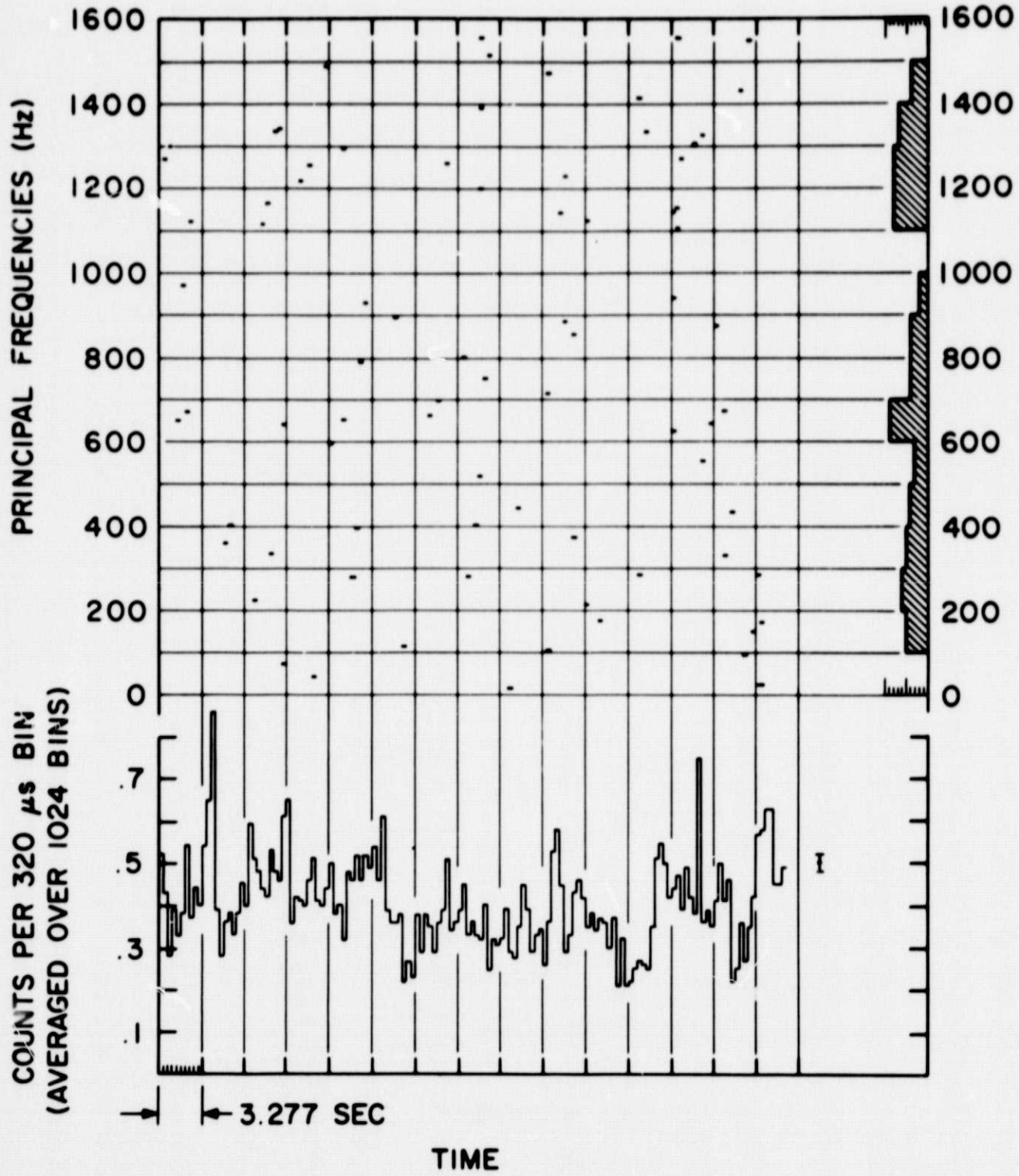
PRINCIPAL FREQUENCIES (Hz)
1600
1400
1200
1000
800
600
400
200
0
COUNTS PER 320 μs BIN
(AVERAGED OVER 1024 BINS)
.7
.5
.3
.1
3.277 SEC
TIME

Figure 16

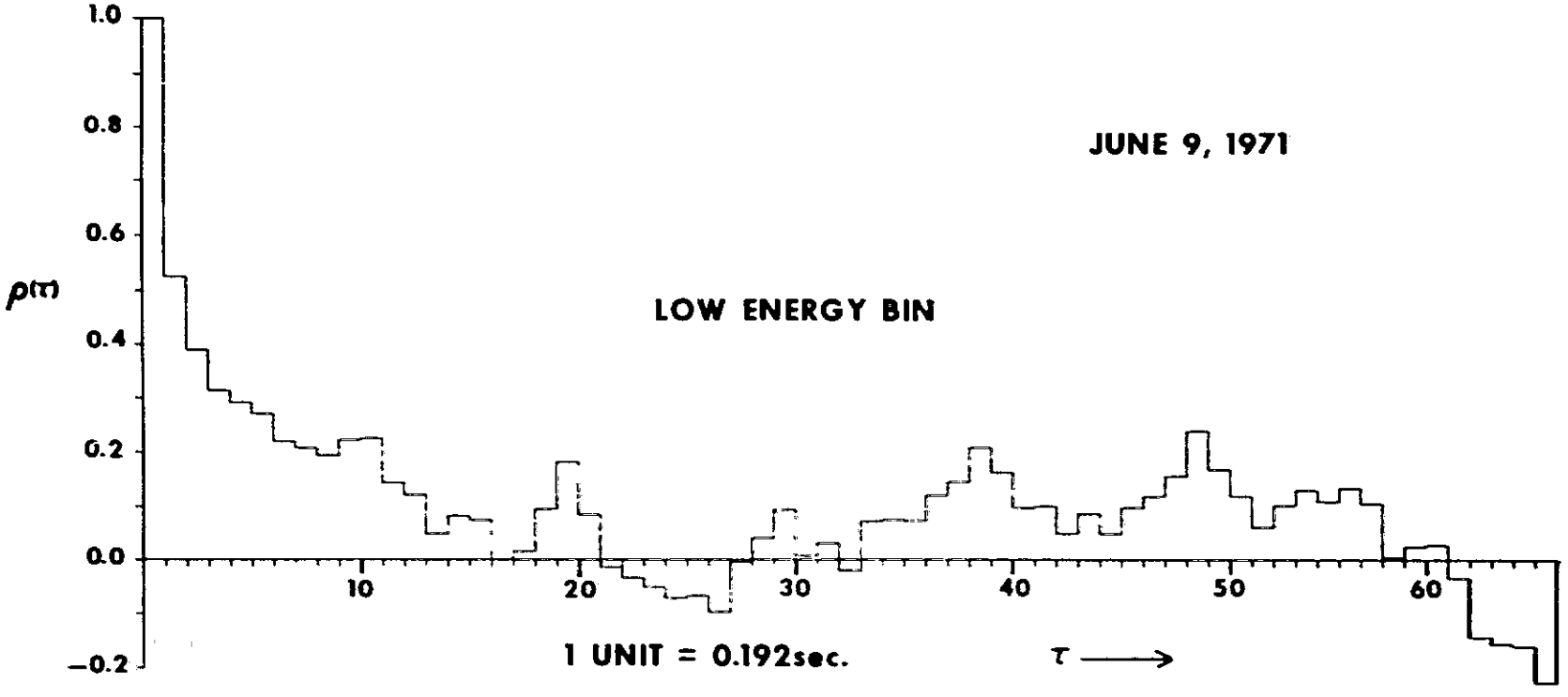
1.0
0.8
0.6
ρ(τ)
0.4
0.2
0.0
−0.2
JUNE 9, 1971
LOW ENERGY BIN
10
20
30
40
50
60
1 UNIT = 0.192sec.
τ ⟶

Figure 17

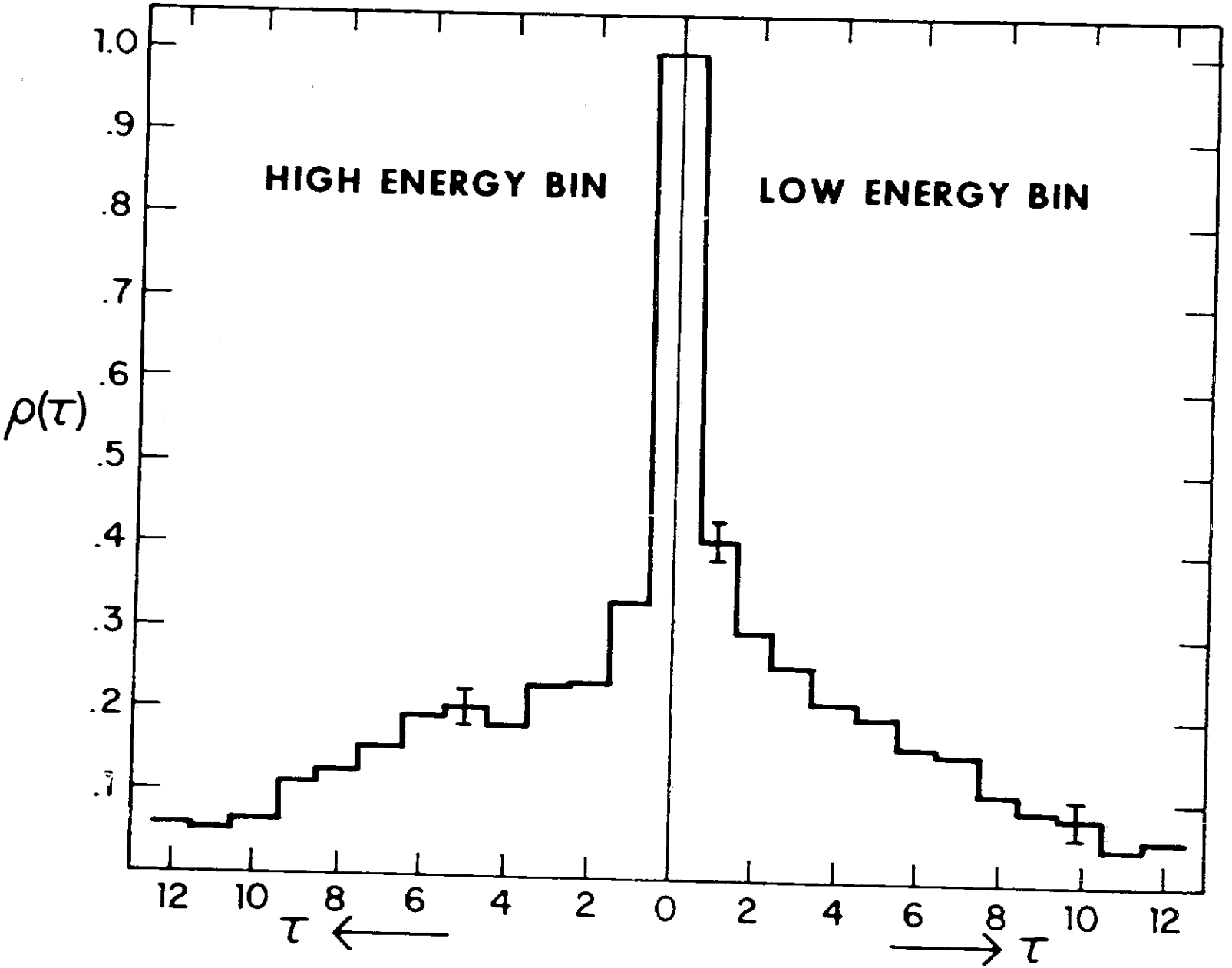
HIGH ENERGY BIN
LOW ENERGY BIN
ρ(τ)
1.0
.9
.8
.7
.6
.5
.4
.3
.2
.1
12 10 8 6 4 2 0 2 4 6 8 10 12
τ
τ

Figure 18

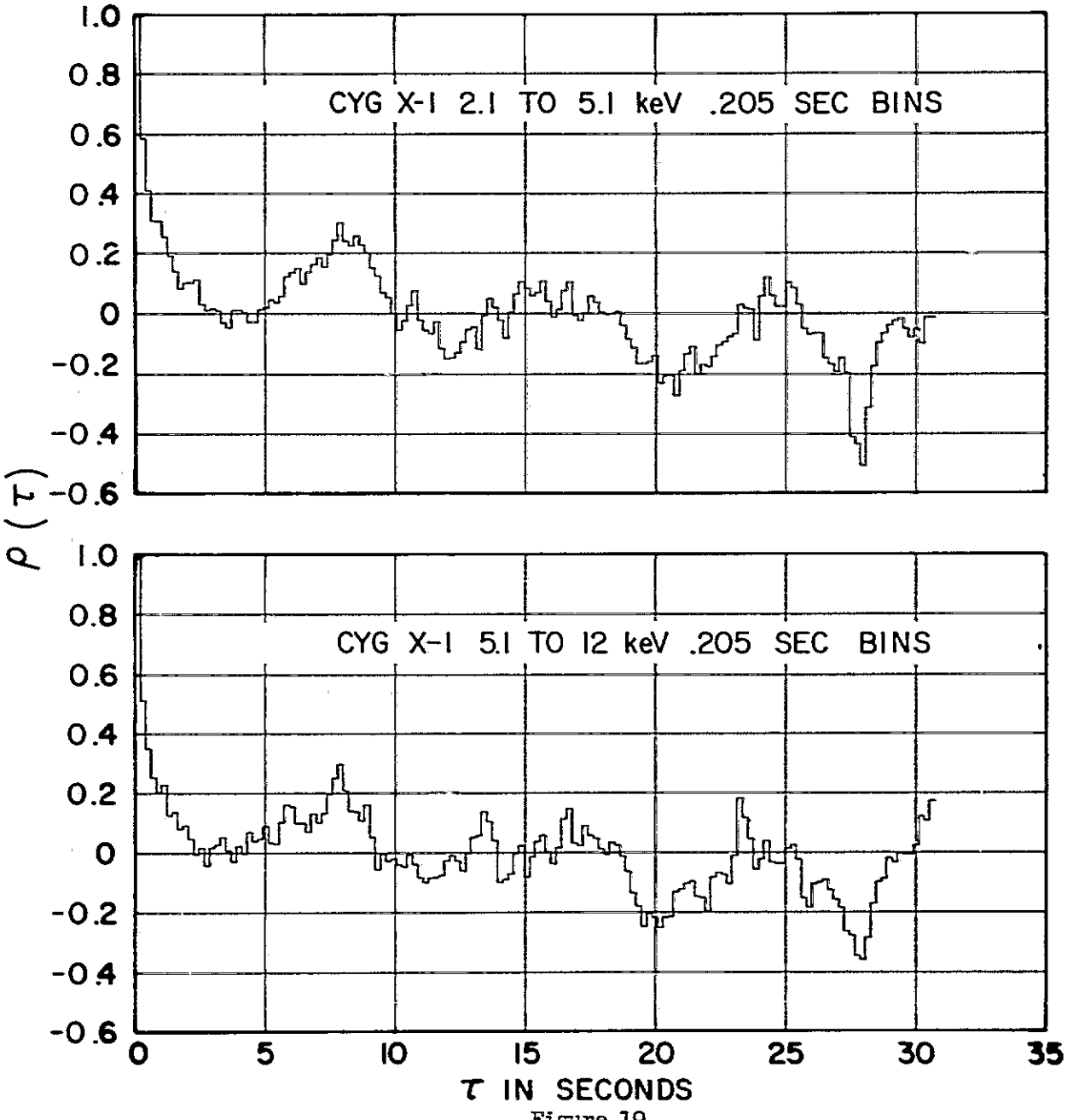
CYG X-1 2.1 TO 5.1 keV .205 SEC BINS
CYG X-1 5.1 TO 12 keV .205 SEC BINS
ρ (τ)
1.0
0.8
0.6
0.4
0.2
0
-0.2
-0.4
-0.6
0
5
10
15
20
25
30
35
τ IN SECONDS

Figure 19

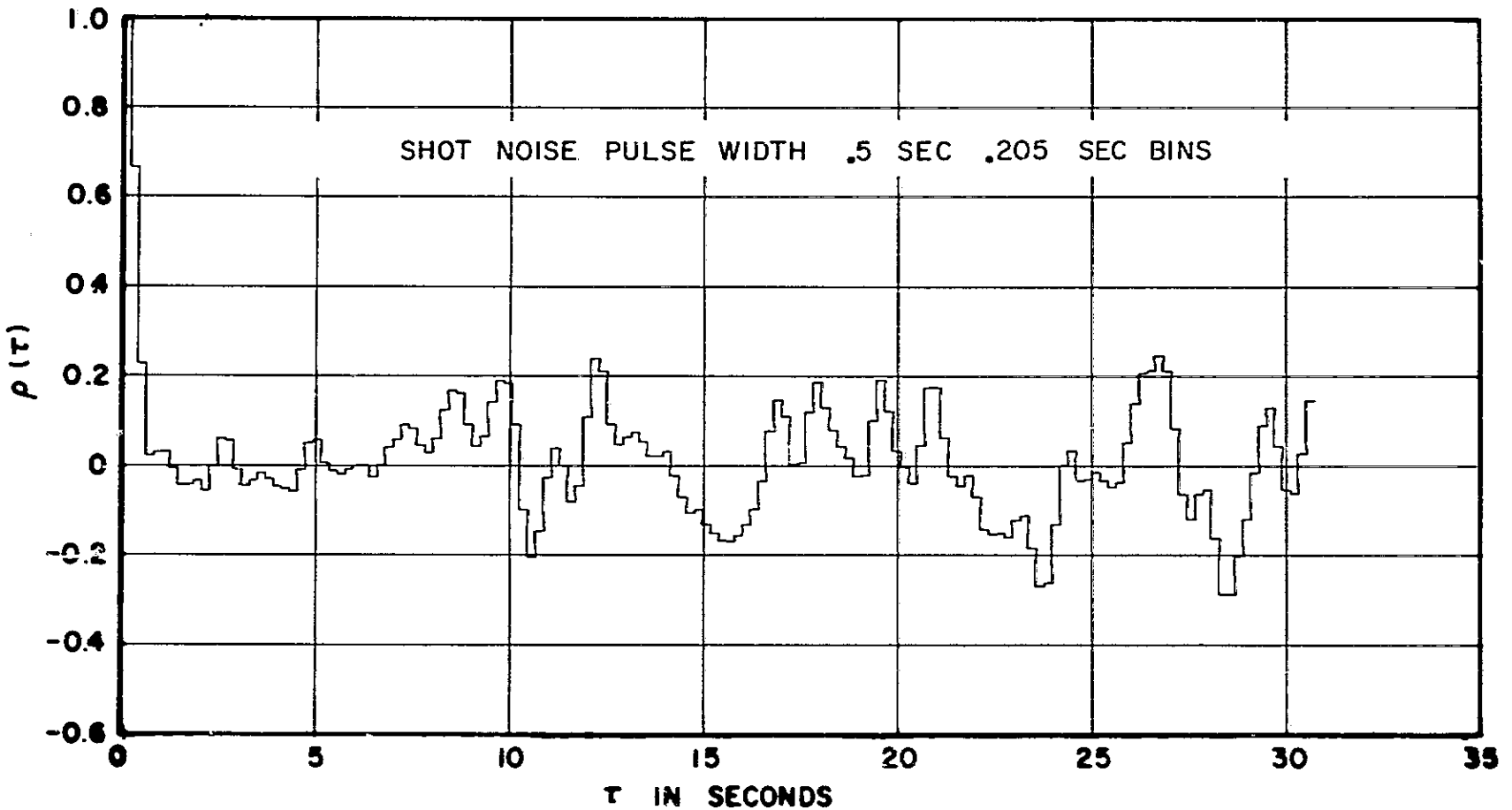
SHOT NOISE PULSE WIDTH .5 SEC .205 SEC BINS
ρ(τ)
1.0
0.8
0.6
0.4
0.2
0
-0.2
-0.4
-0.6
0
5
10
15
20
25
30
35
τ IN SECONDS

Figure 20

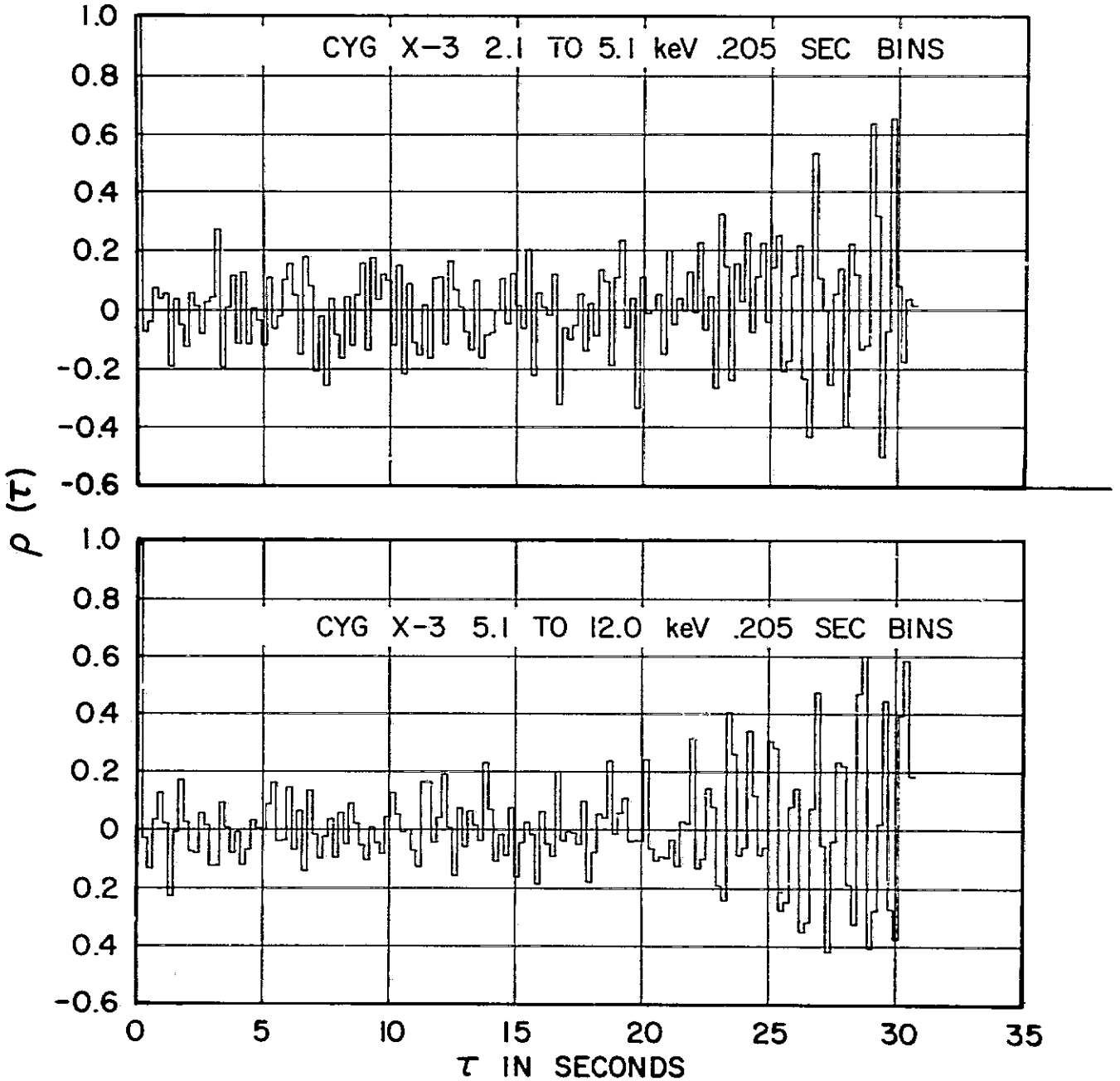
CYG X-3 2.1 TO 5.1 keV .205 SEC BINS
CYG X-3 5.1 TO 12.0 keV .205 SEC BINS
ρ (τ)
1.0
0.8
0.6
0.4
0.2
0
-0.2
-0.4
-0.6
0
5
10
15
20
25
30
35
τ IN SECONDS

Figure 21

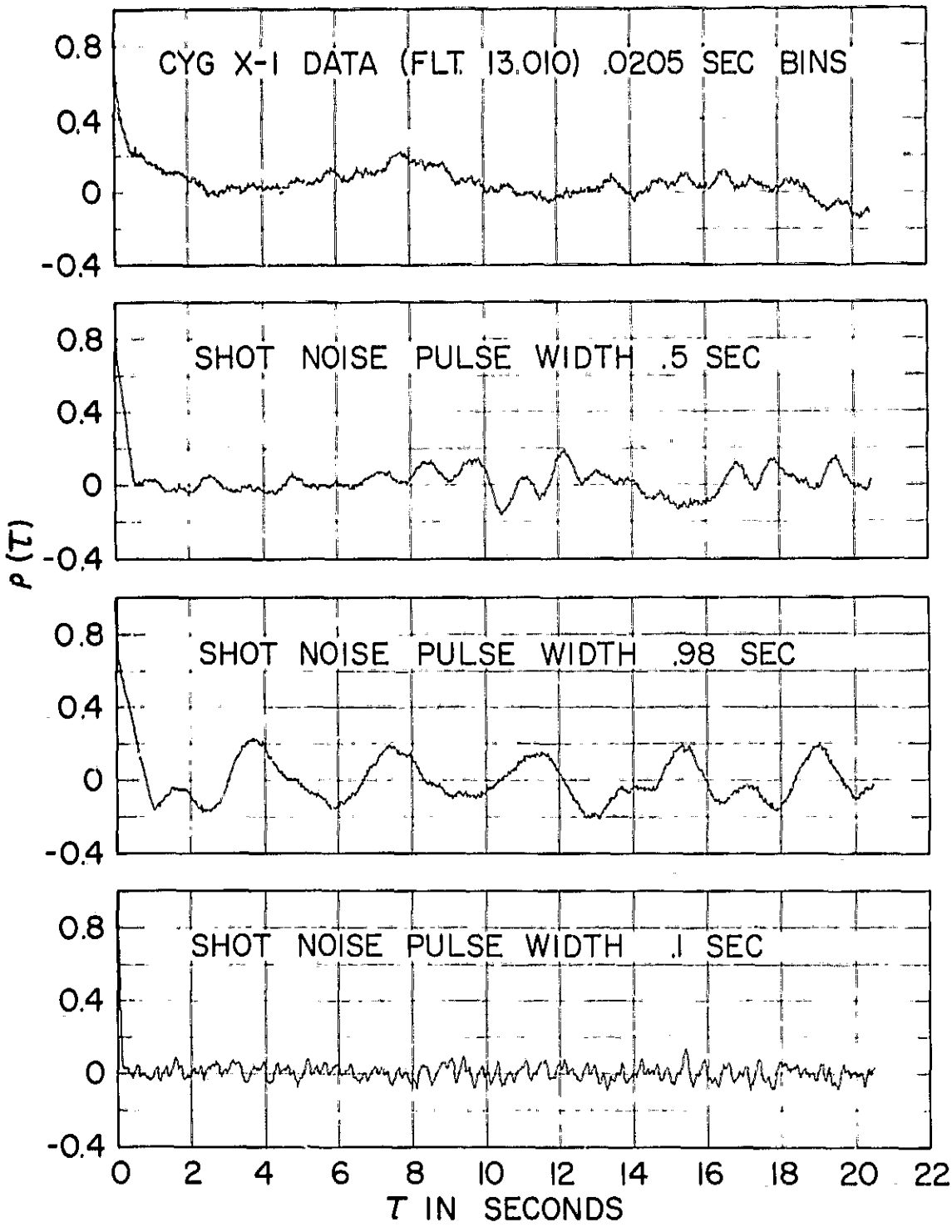
CYG X-1 DATA (FLT. 13.010) .0205 SEC BINS
SHOT NOISE PULSE WIDTH .5 SEC
SHOT NOISE PULSE WIDTH .98 SEC
SHOT NOISE PULSE WIDTH .1 SEC
0.8
0.4
0
-0.4
ρ(τ)
0
2
4
6
8
10
12
14
16
18
20
22
τ IN SECONDS

Figure 22

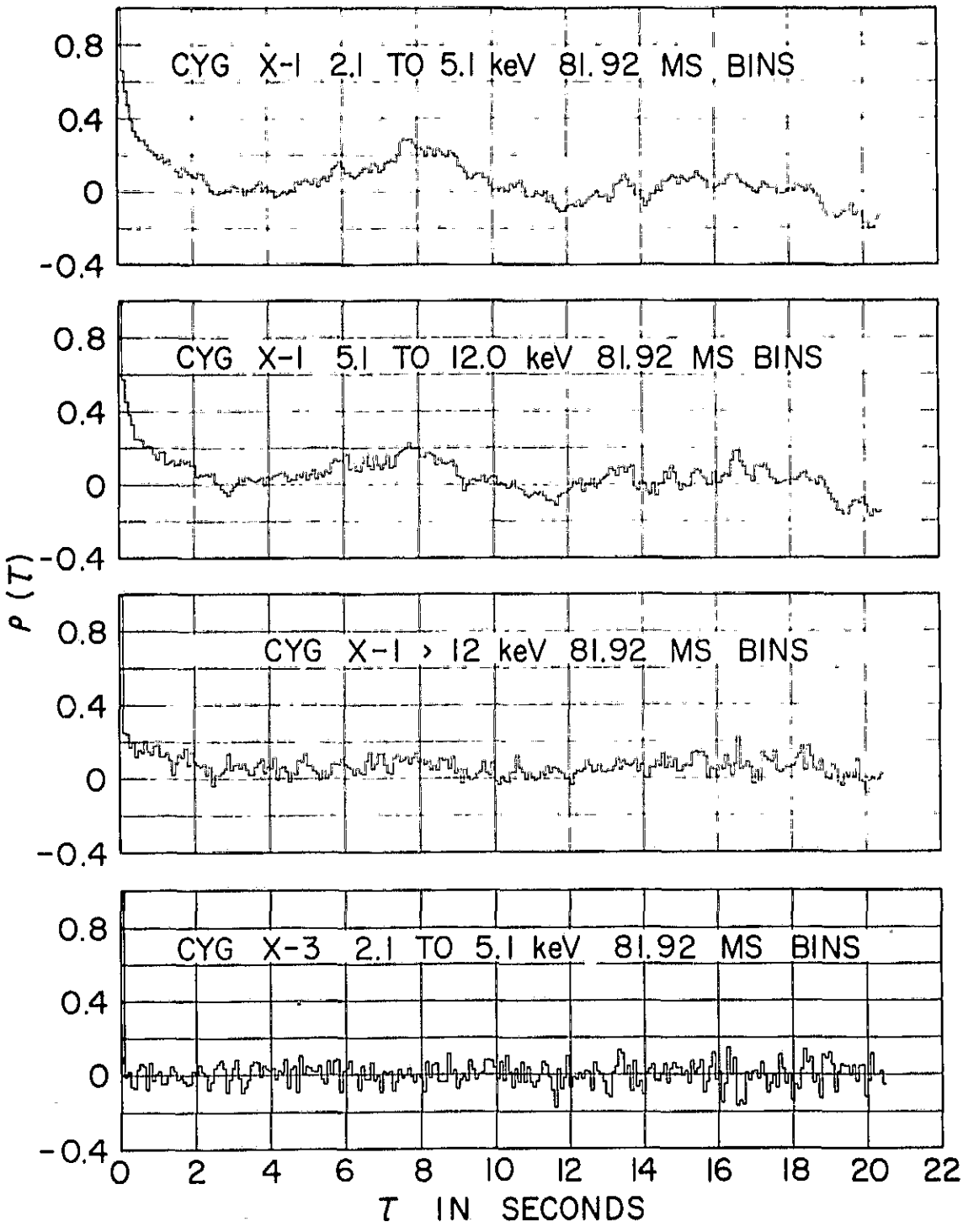
CYG X-1 2.1 TO 5.1 keV 81.92 MS BINS
CYG X-1 5.1 TO 12.0 keV 81.92 MS BINS
CYG X-1 > 12 keV 81.92 MS BINS
CYG X-3 2.1 TO 5.1 keV 81.92 MS BINS
0.8
0.4
0
-0.4
P (T)
0 2 4 6 8 10 12 14 16 18 20 22
T IN SECONDS

Figure 23

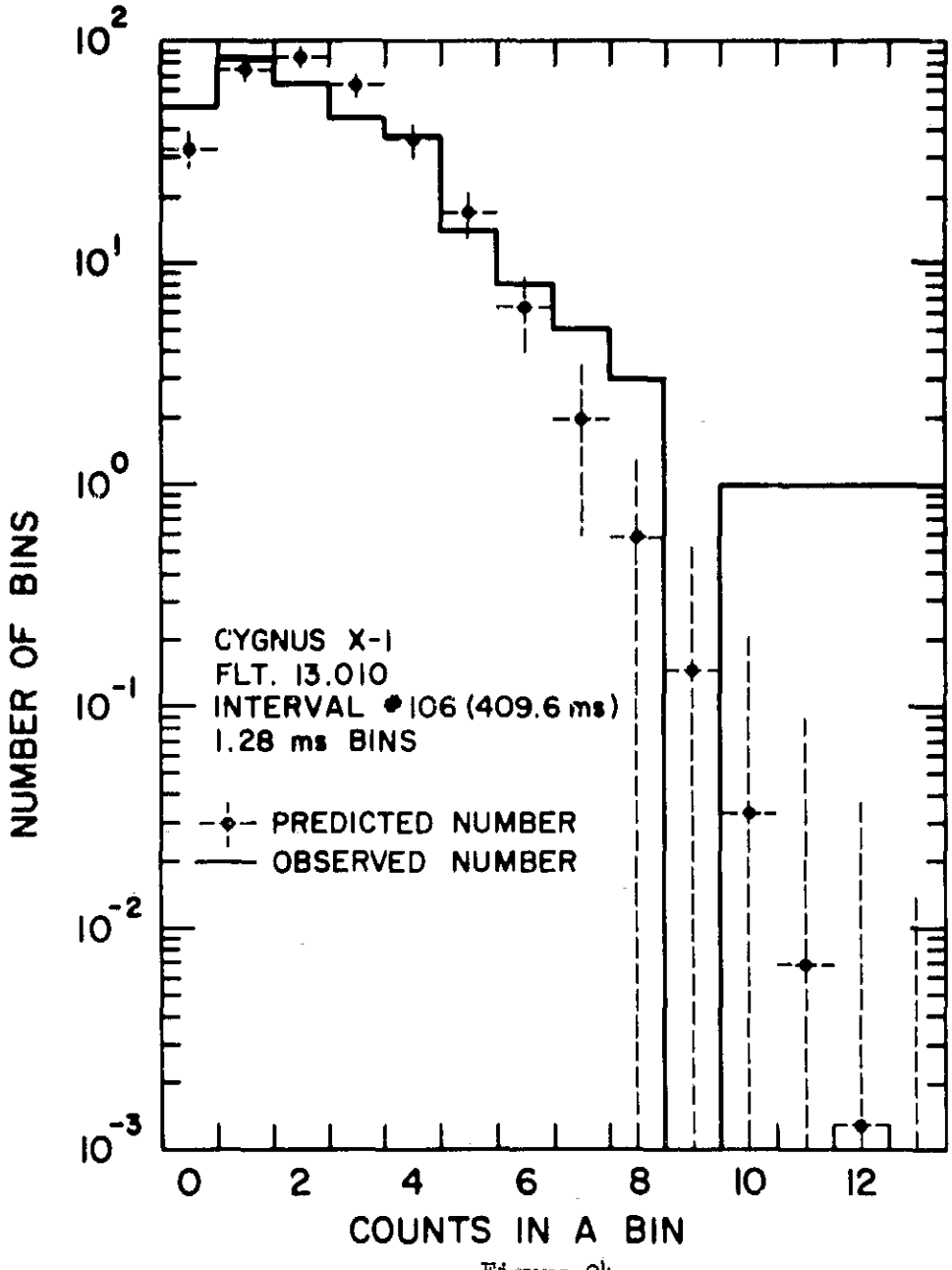
NUMBER OF BINS
10^2
10^1
10^0
10^{-1}
10^{-2}
10^{-3}
CYGNUS X-1
FLT. 13.010
INTERVAL #106 (409.6 ms)
1.28 ms BINS
PREDICTED NUMBER
OBSERVED NUMBER
0
2
4
6
8
10
12
COUNTS IN A BIN

Figure 24

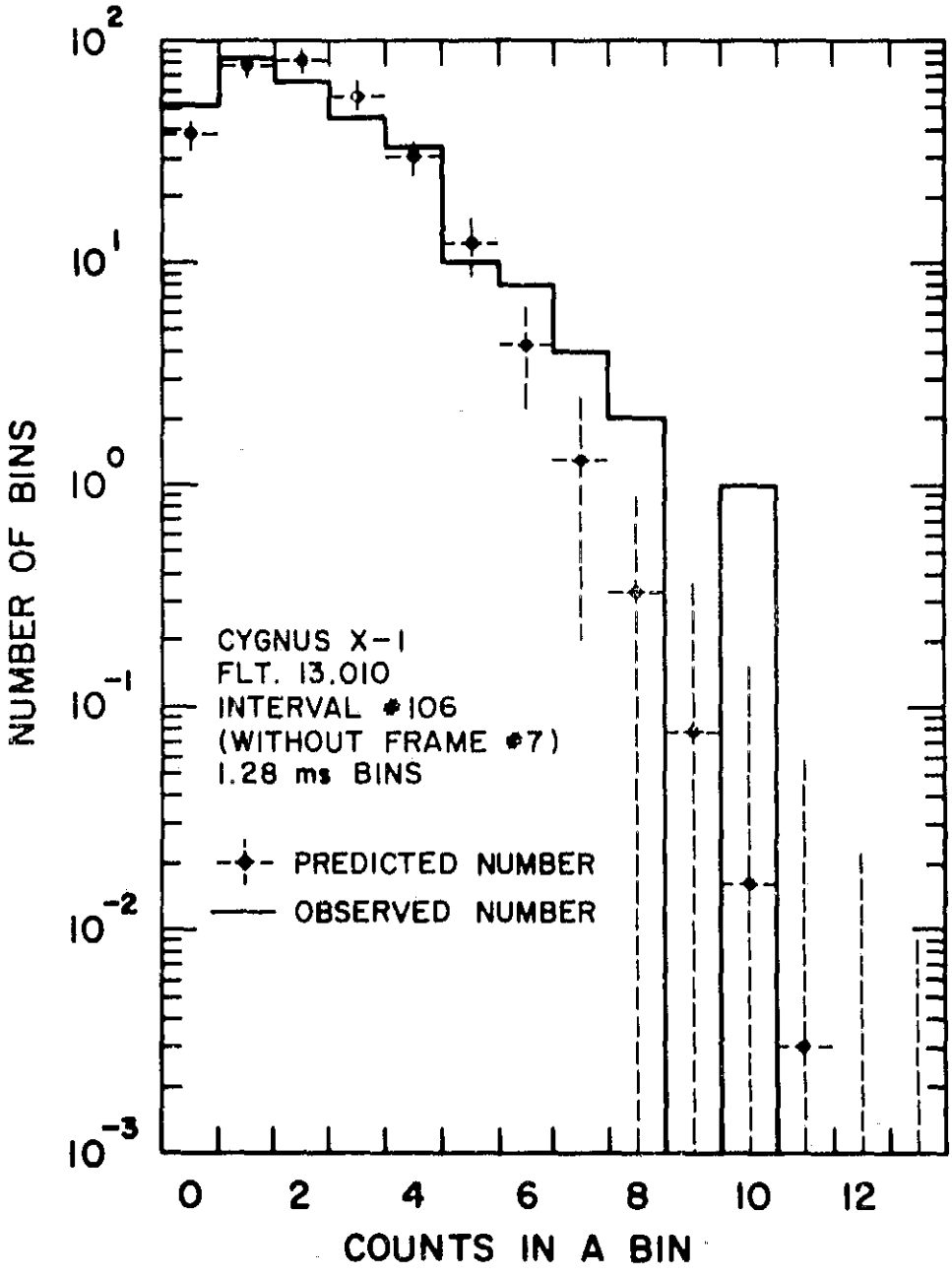
NUMBER OF BINS
10^2
10^1
10^0
10^{-1}
10^{-2}
10^{-3}
CYGNUS X-1
FLT. 13.010
INTERVAL #106
(WITHOUT FRAME #7)
1.28 ms BINS
PREDICTED NUMBER
OBSERVED NUMBER
0
2
4
6
8
10
12
COUNTS IN A BIN

Figure 25

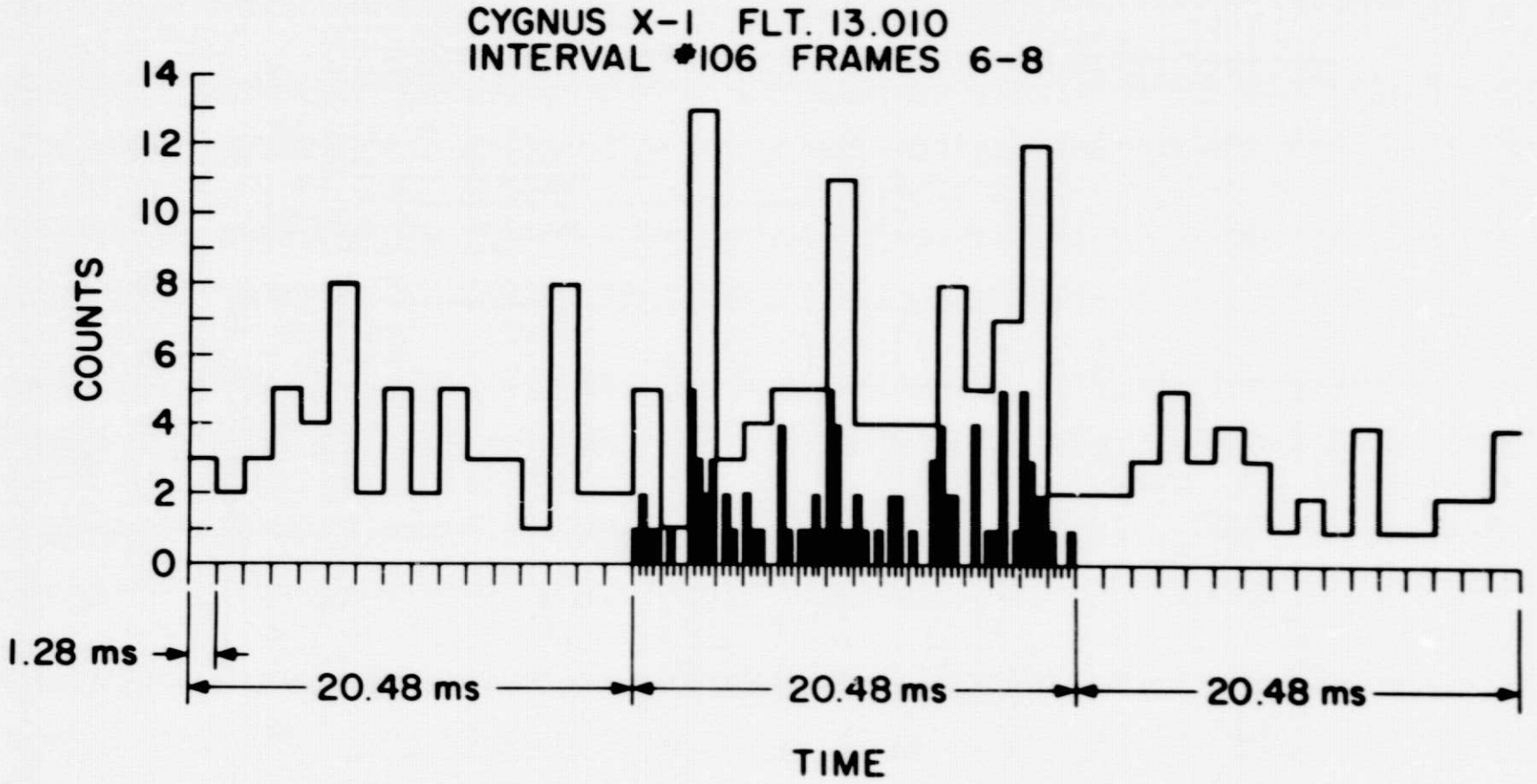

Figure 26

NASA-GSFC